PNNL-19778

U.S. DEPARTMENT OF ENERGY

Prepared for the U.S. Department of Energy
Under Contract DE-AC05-76RL01830

Removing Phosphate from Hanford High-Phosphate Tank Wastes: FY 2010 Results

GJ Lumetta
JC Braley
MK Edwards
O Qafoku
AR Felmy
JC Carter
PJ MacFarlan

September 2010

Pacific Northwest NATIONAL LABORATORY

Proudly Operated by Battelle Since 1965

PACIFIC NORTHWEST NATIONAL LABORATORY
operated by
BATTELLE
for the
UNITED STATES DEPARTMENT OF ENERGY
under Contract DE-AC05-76RL01830

Printed in the United States of America

Available to DOE and DOE contractors from the
Office of Scientific and Technical Information,
P.O. Box 62, Oak Ridge, TN 37831-0062;
ph: (865) 576-8401
fax: (865) 576 5728
email: reports@adonis.osti.gov

Available to the public from the National Technical Information Service,
U.S. Department of Commerce, 5285 Port Royal Rd., Springfield, VA 22161
ph: (800) 553-6847
fax: (703) 605-6900
email: orders@nits.fedworld.gov
online ordering: http://www.ntis.gov/ordering.htm

PNNL-19778

Removing Phosphate from Hanford High-Phosphate Tank Wastes: FY 2010 Results

GJ Lumetta
JC Braley
MK Edwards
O Qafoku
AR Felmy
JC Carter
PJ MacFarlan

September 2010

Prepared for
the U.S. Department of Energy
under Contract DE-AC05-76RL01830

Pacific Northwest National Laboratory
Richland, Washington 99352

Summary

The U.S. Department of Energy (DOE) is responsible for environmental remediation at the Hanford Site in Washington State, a former nuclear weapons production site. Retrieving, processing, immobilizing, and disposing of the 2.2×10^5 m^3 of radioactive wastes stored in the Hanford underground storage tanks dominates the overall environmental remediation effort at Hanford. The cornerstone of the tank waste remediation effort is the Hanford Tank Waste Treatment and Immobilization Plant (WTP). As currently designed, the capability of the WTP to treat and immobilize the Hanford tank wastes in the expected lifetime of the plant is questionable. For this reason, DOE has been pursuing supplemental treatment options for selected wastes. If implemented, these supplemental treatments will route certain waste components to processing and disposition pathways outside of WTP and thus will accelerate the overall Hanford tank waste remediation mission.

One waste component of particular concern is phosphorus. There is a relatively low tolerance for P in the high-level waste (HLW) melter in the WTP. In this report, we examine one concept for processing high-phosphorus Hanford tank sludge solids in such a way that the phosphorus from these wastes does not enter the WTP. In this concept, the high-phosphate waste is retrieved from the waste tank and is leached with aqueous NaOH. This leaching could be performed in a double-shell tank or in the course of the retrieval process if NaOH solution is used to retrieve the sludge solids. After leaching, a solid/liquid separation is performed. The HLW solids are either returned to the tank farm for interim storage or passed on directly to WTP for immobilization in borosilicate glass. The leachate solution is treated with CaO (lime), which will remove the phosphate from solution, most probably as hydroxyapatite, $Ca_5(OH)(PO_4)_3$. The solid hydroxyapatite (and/or other calcium phosphate phases) is a very thermodynamically stable phase and could be readily mixed with cement to form a stable LAW waste form for onsite disposal. The NaOH liberated during the CaO treatment can be recycled either to the caustic leaching vessel or back to the tank farm for use in retrieval.

Based on the results presented in this report, this approach appears to be a viable option for separating phosphate from the Hanford bismuth phosphate sludge waste before transferring this waste to the WTP for immobilization. The chemistry involved—metathesis of insoluble phosphate compounds to sodium phosphate and subsequent precipitation of calcium phosphate phases—is sufficiently robust that it can be implemented under a variety of conditions. The specific operating conditions can be chosen based on engineering requirements. A number of recommendations are provided for further development of this technology.

Acronyms

ALARA	as low as reasonably achievable
DI	deionized (water)
DOE	U.S. Department of Energy
EDS	electron dispersive spectroscopy
ESP	Environmental Simulation Program
FTIR	Fourier transform infrared
HLW	high-level waste
ICP	inductively coupled plasma
LAW	low-activity waste
MSE	mixed-solvent electrolyte
OES	optical emission spectroscopy
PNNL	Pacific Northwest National Laboratory
PSD	particle-size distribution
SEM	scanning electron microscopy
TEM	transmission electron microscopy
TGA	thermogravimetric analysis
WTP	Hanford Tank Waste Treatment and Immobilization Plant
XRD	X-ray diffraction

Contents

Figures

Tables

1.0 Introduction

The U.S. Department of Energy (DOE) is responsible for environmental remediation at former nuclear weapons production sites. The Hanford Site in Washington State represents one of the most daunting challenges to the DOE in fulfilling its environmental remediation mission. Although there are a number of aspects to the Hanford remediation effort, retrieving, processing, immobilizing, and disposing of the 2.2×10^5 m^3 of radioactive wastes stored in the Hanford underground storage tanks dominates the overall effort (Certa et al. 2008). The cornerstone of the tank waste remediation effort is the Hanford Tank Waste Treatment and Immobilization Plant (WTP), which is currently under construction and is scheduled to begin full radioactive operations in 2019. As currently designed, the capability of the WTP to treat and immobilize the Hanford tank wastes in the expected lifetime of the plant is questionable. For this reason, DOE has been pursuing supplemental treatment options for selected wastes. If implemented, these supplemental treatments will route certain waste components to processing and disposition pathways outside of WTP and thus will accelerate the overall Hanford tank waste remediation mission.

One waste component of particular concern is phosphorus. There is a relatively low tolerance for P in the high-level waste (HLW) melter in the WTP. For this reason, considerable effort has been devoted to investigating caustic leaching methods for removing P from the HLW tank sludge solids (Lumetta et al. 1998, 2002, 2008, 2009a). These previous studies have shown that, in most cases, caustic leaching is an effective means to remove P from the HLW solids. However, the previous work was done in the context of the WTP concept. That is, it was envisioned that the HLW solids would be leached with caustic, and the resulting leachate solution containing the P would then be processed through ion exchange to remove ^{137}Cs and immobilized in the low-activity waste (LAW) borosilicate glass waste form. On the other hand, an optimized flowsheet for processing high-phosphate wastes in the WTP has not been developed (most flowsheet work for WTP has been focused on removing Al from high-Al wastes). It is reasonable to examine whether there are other options for managing the P from the Hanford tank sludge solids that route this element to a disposition that does not require it to flow through the WTP.

In this report, we examine one concept for processing high-phosphorus Hanford tank sludge solids. Figure 1.1 schematically summarizes the concept. The high-phosphate waste is retrieved from the waste tank and is leached with aqueous NaOH. It should be noted that the waste could be leached in a double-shell tank or in the course of the retrieval process if NaOH solution is used to retrieve the sludge solids. After leaching, a solid/liquid separation is performed. The HLW solids are either returned to the tank farm for interim storage (as illustrated in Figure 1.1), or passed on directly to WTP for immobilization in borosilicate glass. The leachate solution is treated with lime, which will remove the phosphate from solution, most probably as hydroxyapatite:

$$3Na_3PO_4(aq) + 5CaO(s) + 5H_2O \rightarrow Ca_5(OH)(PO_4)_3(s) + 9NaOH(aq) \quad (1.1)$$

The solid hydroxyapatite (and/or other calcium phosphate phases) is a very thermodynamically stable phase and could be readily mixed with cement to form a stable LAW waste form for onsite disposal.[(a)] In this manner, the P can be routed for disposal without being processed through the WTP. The NaOH liberated in Eq. 1.1 can be recycled either to the caustic leaching vessel or back to the tank farm for use in

(a) Regulatory approval of this waste form would need to be obtained.

retrieval.[(a)] A similar caustic leaching/Ca precipitation scheme has been investigated for recovering phosphorus from wastewater treatment plant sludges (Stark and Hultman 2003).

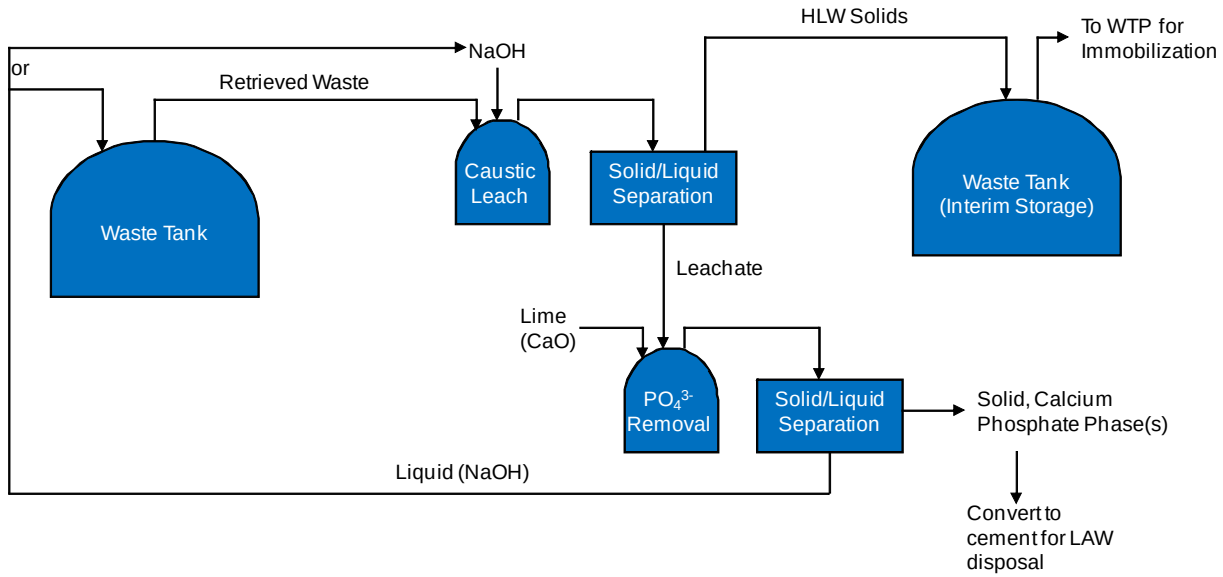

Figure 1.1. Conceptual Illustration of Phosphate Removal from HLW Hanford Tank Sludge Solids. Note: For clarity, solids washing steps have not been shown.

To examine the feasibility of this concept, we undertook a series of investigations using a non-radioactive simulant of a Hanford tank sludge. Sludge waste generated from the Bismuth Phosphate Process (hereafter referred to as *$BiPO_4$ sludge*) is the single largest source of P in the Hanford tank waste, representing an estimated 36% of the total P (Lumetta et al 2009a). For this reason, we focused our efforts on simulating this type of tank waste. In developing the simulant for the $BiPO_4$ sludge, we built upon previous characterization and simulant development efforts (Lumetta et al. 2009b). The following are the key tasks undertaken in FY 2010:

1. Developing $BiPO_4$ sludge simulant
2. Performing parametric caustic leaching tests using the simulant to optimize the conditions for phosphate removal from the tank waste solids
3. Testing the treatment of the leachate solutions with lime to remove the P as a stable calcium phosphate phase
4. Improving phosphate solubility models to guide flowsheet design
5. Examining phosphate precipitation and gelling phenomena that pose risks to operation of the process if not properly controlled.

This report summarizes the results of this study and provides recommendations for future development of the phosphate management technology.

(a) It can be anticipated that the leachate solution will contain ^{137}Cs and that this will build up upon continued recycle of the NaOH solution. It might be necessary to remove this ^{137}Cs at some point, which could be done either in the WTP or with a supplemental ^{137}Cs removal capability.

2.0 Experimental

In this section, we describe the experimental methods that were used in simulant development, parametric leaching experiments, lime treatment, and the study of fundamental phosphate solubility equilibria.

2.1 $BiPO_4$ Sludge Simulant Development

Two approaches were pursued in developing the $BiPO_4$ sludge simulant: 1) mimicking the plant operations that produced the waste and 2) precipitating iron(III) phosphate.

2.1.1 Mimic of Plant Operations

Deionized (DI) water (50 mL) was placed in a beaker, and 10.95 mL of concentrated (16 M) HNO_3 was added. While stirring, the following salts were added in the order listed:

Order of Addition	*Chemical*	*FW*	*Amount Added, g*
1	$Fe_2(SO_4)_3 \cdot xH_2O$	555.4[(a)]	2.57
2	$(NH_4)_2SO_4$	132.1	0.87
3	$Bi(NO_3)_3 \cdot 5H_2O$	485.1	0.74
4	$Cr(NO_3)_3 \cdot 9H_2O$	400.1	0.59
5	$NaNO_3$	84.99	0.43
6	NH_4NO_3	80.04	2.08
7	$(NH_4)_2SiF_6$	178.1	3.66

Concentrated (13.7 M, 4.75 mL) H_3PO_4 was added, and the mixture was stirred for approximately 2 h. The solution was diluted to 100 mL with DI water. Fifty milliliters of the resulting solution was transferred to a plastic bottle, and 6.6 mL of 50 wt% NaOH was added dropwise with stirring. During this process, the temperature did not exceed 60°C. After cooling to ambient temperature, the slurry was divided between two 50-mL centrifuge cones and centrifuged, and the liquid was decanted. The solids were washed three times with DI water, centrifuging and decanting after each washing step. The washed solids were collected and air dried.

(a) Formula weight for iron(III) sulfate estimated from the minimum assay of 72% $Fe_2(SO_4)_3$ listed on the product label; i.e., x ~ 8.6.

2.1.2 Precipitation of Iron(III) Phosphate

A 0.22 M stock solution of Na_3PO_4 was prepared by dissolving 16.39 g (0.0431 mole) $Na_3PO_4 \cdot 12H_2O$ in DI water and diluting to 200 mL. A 1.0 M stock solution of $Fe(NO_3)_3$ was prepared by dissolving 40.4 g (0.1 mole) $Fe(NO_3)_3 \cdot 9H_2O$ in DI waster and diluting to 100 mL. These solutions were used to precipitate iron(III) phosphate under conditions of variable temperature, pH, and iron concentration. The influence of Bi(III) was also explored.

Variable Temperature. The 0.22 M Na_3PO_4 solution (10 mL, 2.2 mmole) was placed in a 20 ML plastic scintillation vial and brought to temperature (25, 40, 60, or 80°C) using an aluminum heating block. Once at temperature, 5.5 mL (5.5 mmole) of the 1.0 M $Fe(NO_3)_3$ solution was added dropwise while continuously mixing on a rotary shaker. The resulting solids were collected by filtration, washed with DI water, and air-dried.

Variable pH. The 0.22 M Na_3PO_4 solution (10 mL, 2.2 mmole) was placed in a 20-mL plastic scintillation vial and adjusted to the desired pH. In most cases, this required adding of H_3PO_4 because the pH of the 0.22 M Na_3PO_4 solution was 11.5. In this way, portions of the Na_3PO_4 solution were adjusted to pH 7, 9, and 11. Originally, one test was planned at pH 13, but upon adjusting the solution with NaOH, a precipitate began to form at pH approximately 12.3; the NaOH addition was stopped at that point. To each of the pH-adjusted Na_3PO_4 solutions, 5.5 mL (5.5 mmole) of the 1.0 M $Fe(NO_3)_3$ solution was added dropwise with stirring. The resulting solids were collected by filtration, washed with DI water, and air-dried.

Variable Iron Concentration. Three dilutions of the 1 M $Fe(NO_3)_3$ solution were made: 2× (5.5 mL 1 M $Fe(NO_3)_3$ + 5.5 mL DI water), 10× (5.5 mL 1 M $Fe(NO_3)_3$ + 49.5 mL DI water), and 50× (5.5 mL 1 M $Fe(NO_3)_3$ + 269.5 mL DI water). These solutions were added dropwise with stirring to 10 mL each of the 0.22 M Na_3PO_4 solution. Under these conditions, the Fe concentration was variable, but the molar ratio of P-to-Fe was kept constant at 0.4. The solids were filtered, washed with DI water, and air-dried.

With Bismuth Present. $Bi(NO_3)_3 \cdot 5H_2O$ (0.78 g, 1.6 mmole) was dissolved in 5.5 mL of 1.0 M $Fe(NO_3)_3$ (5.5 mmole). This solution was added dropwise with stirring to 20 mL of 0.22 M Na_3PO_4 solution (4.4 mmole). The solids were filtered, washed with DI water, and air-dried.

Variable Temperature at pH 12.3. A 0.5 M solution of Na_3PO_4 was prepared by dissolving 19.007 g (0.050 mole) $Na_3PO_4 \cdot 12H_2O$ in DI water and diluting to 100 mL. This solution was adjusted to pH 12.3 with NaOH. A 1.0 M solution of $Fe(NO_3)_3$ was prepared by dissolving 10.1 g (0.025 mole) $Fe(NO_3)_3 \cdot 9H_2O$ in DI water and diluting to 25 mL. Four 10-mL portions of the pH-adjusted 0.22 M Na_3PO_4 solution were transferred to 20-mL plastic scintillation vials. Each portion of Na_3PO_4 solution was brought to the desired temperature (25, 40, 60, or 80°C) using an aluminum heating block. Once at temperature, 5.5 mL (5.5 mmole) of the 1.0 M $Fe(NO_3)_3$ solution was added dropwise while continuously mixing on a rotary shaker.. The resulting solids were collected by filtration, washed with DI water, and air-dried.

2.1.3 Scale-up of pH 12 Iron(III) Phosphate Simulant

A 0.5 M solution of Na_3PO_4 was prepared by dissolving 38.161 g (0.100 mole) $Na_3PO_4 \cdot 12H_2O$ in DI water and diluting to 200 mL. This solution was adjusted to pH 12.5 with NaOH. The 1.0 M solution of

$Fe(NO_3)_3$ was prepared by dissolving 60.710 g (0.150 mole) $Fe(NO_3)_3 \cdot 9H_2O$ in DI water and diluting to 150 mL. A portion of the 1 M $Fe(NO_3)_3$ solution (110 mL, 0.11 mole) was added to the pH-adjusted Na_3PO_4 solution with stirring. The solid product was filtered, washed with water, and allowed to air dry, yielding 30.68 g of product. For further investigations, a portion of the simulant was ground with a mortar and pestle and passed through a 0.45-µm sieve. A 0.0568-g portion of the simulant was dissolved in 1 mL concentrated HCl and diluted to 15 mL with DI water; this solution was analyzed by inductively coupled plasma-optical emission spectroscopy (ICP-OES) for Na, Fe, and P. Unless otherwise noted, this batch of simulant is what is referred to as the "$BiPO_4$ simulant" throughout this report.

2.2 Parametric Caustic Leaching

2.2.1 Variable NaOH Concentration at Ambient Temperature

Three approximately 0.5-g portions of the $BiPO_4$ simulant were weighed into 60-mL plastic bottles. Deionized water was added along with enough 10 M NaOH to give free hydroxide concentrations of 0.5, 1.0, and 2.0 M after taking into account the reaction of hydroxide with the $FePO_4$ in the simulant. The total volume of leachate solution was chosen so that the sodium phosphate solubility (0.067 M) would not be exceeded in the 2 M NaOH case; the volume required was 85 mL/g simulant. The leaching mixtures were stirred for a specified length of time. Then they were centrifuged, and the amount of phosphate in solution was monitored with Raman spectroscopy. After recording the Raman spectrum of the solution phase, the leachate sample was returned to the reaction vessel, and stirring was continued. Raman spectra were obtained at 15, 60, 120, and 175 min. Following the last Raman sampling, the solids were collected by filtration, washed with water, and allowed to air-dry. The leaching and washing solutions were combined and analyzed for Fe, Na, and P by ICP-OES.

2.2.2 Variable Temperature at Constant 0.5 M NaOH

Three 0.5-g portions of the $BiPO_4$ simulant were weighed into 60-mL plastic bottles, and to each of these was added 39.9 mL DI water and 2.77 mL of 10 M NaOH. The amount of NaOH used was such that the final NaOH concentration would be 0.5 M if all the phosphate in the simulant were converted to sodium phosphate. After adding NaOH, each reaction bottle was placed in a temperature-controlled aluminum heating block and mixed with an orbital shaker at the desired temperature (25, 40, or 60°C) for 15 min. The mixtures were immediately filtered through 0.45-µm nylon filters. The filtered solids were washed with water and air dried. The wash solutions were combined with the corresponding leachate solutions, and the combined solutions were analyzed for Fe, Na, and P by ICP- OES. Portions of the solids remaining after leaching were dissolved in HCl and also analyzed by ICP-OES.

2.3 Phosphate Removal by Treatment with Lime

2.3.1 First Kinetics Test at Ambient Temperature

Ten milliliters of 0.19 M Na_3PO_4/1 M NaOH solution (1.9 mmole PO_4^{3-}) were mixed by magnetic stirring with 0.1989 g CaO (3.5 mmole Ca). At selected time intervals (5, 15, 30, 60, 90, 120 min), 0.5-mL (0.75-mL at 120 min) portions of the slurry were taken and filtered through a 0.2-µm nylon syringe filter. Aliquots of the clarified liquid were acidified with nitric acid and analyzed by ICP-OES for

Na and P. A sample of the initial 0.15 M Na_3PO_4/1 M NaOH solution was also analyzed for Na and P. The starting 0.15 M Na_3PO_4/1 M NaOH solution and the liquid phase obtained after treatment with CaO for 120 min were titrated with standard HCl to determine the free hydroxide concentration (taken to be the first equivalence point in the titration curve). The remaining solids in the slurry were collected by filtration, washed with DI water, and air-dried.

2.3.2 Kinetics Test at 40°C

Ten milliliters of 0.18 M Na_3PO_4/1 M NaOH solution (1.8 mmole PO_4^{3-}) were mixed using an orbital shaker with 0.2051 g CaO (3.7 mmole Ca) at 40°C. The temperature was maintained with an Al heating block secured to the orbital shaker. At selected time intervals (15, 60, 120, 240, and 360 min), 0.5-mL (0.75-mL at 120 min) portions of the slurry were taken and filtered through a 0.2-µm nylon syringe filter. All other aspects of this test were analogous to that described in Section 2.3.1.

2.3.3 Second Kinetics Test at Ambient Temperature

The second kinetics test at ambient temperature was essentially identical to the first experiment (Section 2.3.1), but twice as much CaO was used. Ten milliliters of 0.18 M Na_3PO_4/1 M NaOH solution (1.8 mmole PO_4^{3-}) were mixed with 0.4014 g CaO (7.2 mmole Ca). Samples were taken for analysis as previously described at 5, 15, 30, 60, 90, and 120 min. The remaining solids in the slurry were collected by filtration, washed with DI water, and air-dried. Analyses performed were the same as those described in Section 2.3.1.

2.4 Sequential Phosphate Leaching and Calcium Oxide Treatment Tests

Table 2.1 summarizes the leaching conditions used in the sequential phosphate leaching and calcium oxide treatment tests. Cases 1 and 2 were designed to mimic a process evolution in which the sludge solids are water-washed before leaching, so no salts were added to the $BiPO_4$ simulant. Cases 2 and 3 were designed to mimic conditions in which leaching is performed with no prior washing of the solids. In these latter cases, sodium nitrate, sodium fluoride, and sodium sulfate were added to constitute a more complete "unwashed" $BiPO_4$ simulant. Table 2.2 provides the amounts of $NaNO_3$, NaF, and Na_2SO_4 added per gram of $BiPO_4$ simulant. Enough sodium hydroxide was added to provide 0.5 M, free-hydroxide concentration, assuming consumption of three moles of NaOH per mole of PO_4^{3-} in the simulant solids. The $BiPO_4$ simulant and the 0.5 M NaOH leaching phase were mixed together for 30 minutes on an orbital shaker, and the temperature was maintained with an Al heating block. After leaching, the solids were collected by filtration through a 0.2-µm nylon syringe filter, washed, and air-dried.

Samples were taken of both the leachate solution and the washing solution for ICP-OES determination of Na and P. A 10-mg sample of the $BiPO_4$ simulant was also dissolved in 2% HCl for ICP-OES analysis of Fe, P and Na. The leaching and washing solutions were combined, and a sample was obtained of this solution for a hydroxide determination by pH titration.

Table 2.1. Description of Test Conditions for Phosphate Leaching in the Integrated Phosphate Leaching and Calcium Oxide Treatment Tests

	$NaNO_3$[(a)]	T, °C	V_{NaOH}, mL[(b)]	V_{total}, mL	wt% P
Case 1	0	22	0.83	10	8.0
Case 2	0	60	0.83	10	8.0
Case 3	2.4	22	1.16	25	3.2
Case 4	2.4	60	0.60	10	3.2

(a) Expressed in terms of grams $NaNO_3$ per gram $FePO_4 \cdot 3.4H_2O$
(b) [NaOH] = 10.75 M

Table 2.2. Amounts of Sodium Nitrate, Sodium Fluoride, and Sodium Sulfate Added to the $BiPO_4$ Sludge Simulant for the Integrated Leaching and Calcium Precipitation Tests

	Grams added per gram $BiPO_4$ Sludge Simulant	
Component Added	Case 1, 2 Washed Solids	Case 3,4 Unwashed Solids
$NaNO_3$	0	2.4
NaF	0.2	0.2
$Na_2SO_4 \cdot 10H_2O$	0.5	0.5

The combined leach/wash solution was contacted with four equivalents of calcium oxide relative to phosphate (assuming quantitative dissolution of phosphate during the leaching step) for 60 minutes at 22°C. The solids were again collected by filtration through a 0.2-µm nylon syringe filter, water-washed, and air-dried. Three aliquots of the lime treated solution were obtained: two for ICP-OES analysis of Na, Ca, and P and one for hydroxide determination by acid titration. Portions of the solids remaining after leaching were taken for Raman and Fourier transform infrared (FTIR) analysis. Other solid samples were dissolved in HCl and also analyzed by ICP-OES.

3.0 Results

3.1 $BiPO_4$ Sludge Simulant Development

Because this work is directed at developing the means to separate P from the HLW feed to the WTP, developing the $BiPO_4$ sludge simulant focused on simulating the chemical behavior of P in this type of waste.[(a)] Previous characterization of actual $BiPO_4$ sludge solids, along with preliminary attempts to simulate these solids, suggested that the phosphate component of the solids is best represented by amorphous iron(III) phosphate (Lumetta et al. 2009b). Optimization of the simulant preparation followed two lines of inquiry: 1) mimicking the plant operations that were conducted at Hanford and 2) precipitating iron(III) phosphate by mixing iron(III) nitrate with sodium phosphate. For the latter, a number of parameters were examined, including temperature, pH, the initial Fe concentration, and the presence of Bi^{3+}. FTIR spectroscopy was used as a screening tool to determine how well the simulants matched the actual $BiPO_4$ sludge solids.

3.1.1 Simulant from Mimic of Plant Operations

Figure 3.1 compares the FTIR spectrum of the simulant material obtained by mimicking the Hanford plant operations during the Bismuth Phosphate Process.[(b)] The actual tank waste displays two overlapping bands in the ν_3(P=O) region, one with a peak position at 1000 cm^{-1} and the other appearing as a shoulder at 1050 cm^{-1}. The phosphate band from the plant simulant appears as a single strong band at 1029 cm^{-1}, lying between the two bands observed in the actual waste. There are significant differences between the spectrum of the plant simulant and the actual waste at lower energy, specifically the bands at 702 and 728 cm^{-1} and the sharp bands at 473, 493, and 518 cm^{-1} in the simulant. There are no corresponding bands in the spectrum of the actual waste.

(a) The simulant used in this work was developed only to mimic the phosphate leaching behavior of the Hanford $BiPO_4$ sludge solids. No attempt was made to simulate other features of the waste, such as rheology. Because the simulant was to be used to optimize the conditions for phosphate leaching, minor waste constituents were not included in the simulant. More complex simulants should be considered for further development and scale-up of the process.

(b) HW-23043. 1951. "Flow Sheets and Flow Diagrams of Precipitation Separations Process." Hanford Works, Richland, Washington.

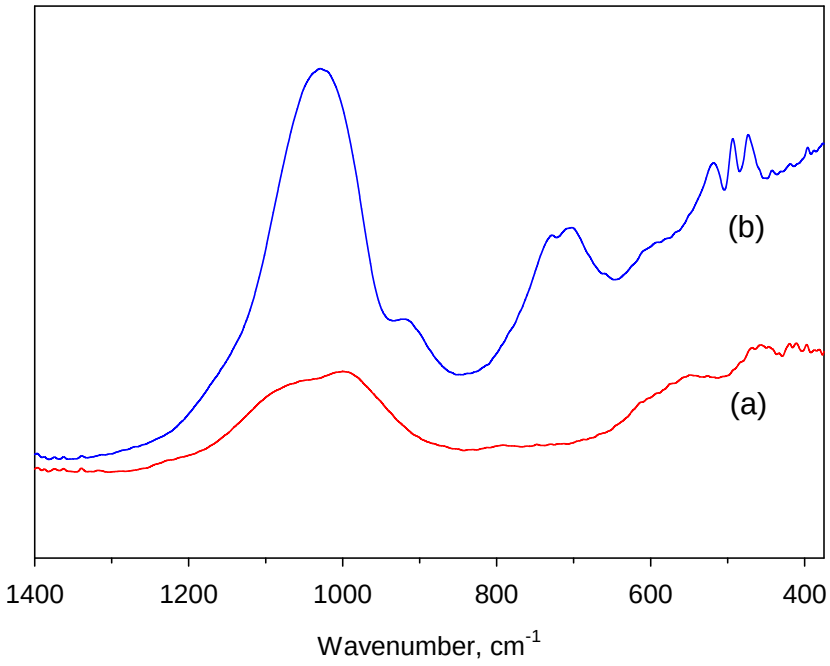

Figure 3.1. Comparison of the FTIR Spectra of a) Actual $BiPO_4$ Sludge (Lumetta et al. 2009b) and b) the Simulant Prepared by Mimicking the Hanford Plant Operations

3.1.2 Simulants from Precipitation of Iron(III) Phosphate

Figure 3.2 shows the FTIR spectra of the iron(III) phosphate simulants prepared by adding iron(III) nitrate solution to sodium phosphate solution at different temperatures. Also shown for comparison is the spectrum of the actual tank waste material. Temperature had no discernable effect on the product formed in this series of precipitation reactions. The FTIR spectra of all of these materials agree reasonably well with the actual tank waste material with the ν_3(P=O) at 1010 cm^{-1}.

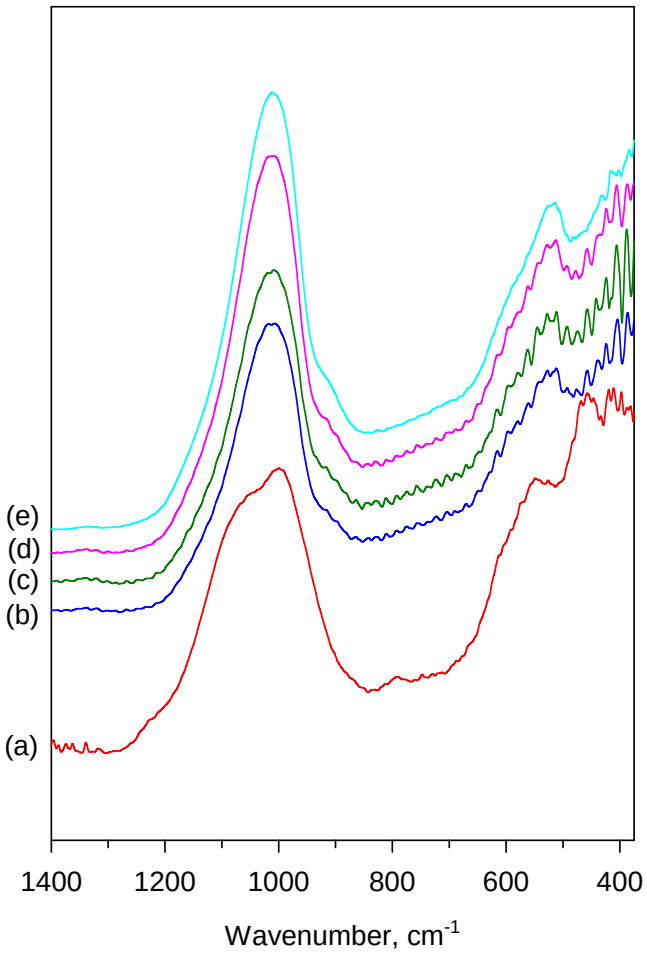

Figure 3.2. FTIR Spectra of Simulants Prepared by Mixing $Fe(NO_3)_3$ and Na_3PO_4 Solutions at Different Temperatures: a) Actual $BiPO_4$ Sludge Tank Waste (Lumetta et al. 2009b), b) 25°C, c) 40°C, d) 60°C, and e) 80°C

Figure 3.3 compares the FTIR spectra of the iron(III) phosphate simulants prepared at different initial pH. The ν_3(P=O) band shifts to lower energy with increasing pH of the starting sodium phosphate solution. The positions of these bands are 1030, 1025, 1018, and 993 cm^{-1} for the pH 7, 9, 11, and 12.3 simulants, respectively. Considering the main ν_3(P=O) band in the actual waste at 1000 cm^{-1}, the simulant prepared at pH 12.3 resembles the actual waste fairly well. This resemblance includes the shape of the spectra at lower energy, e.g., the shoulder at approximately 525 cm^{-1}, which can be assigned to the ν_4(P=O) stretch (Steger and Schmidt 1964).

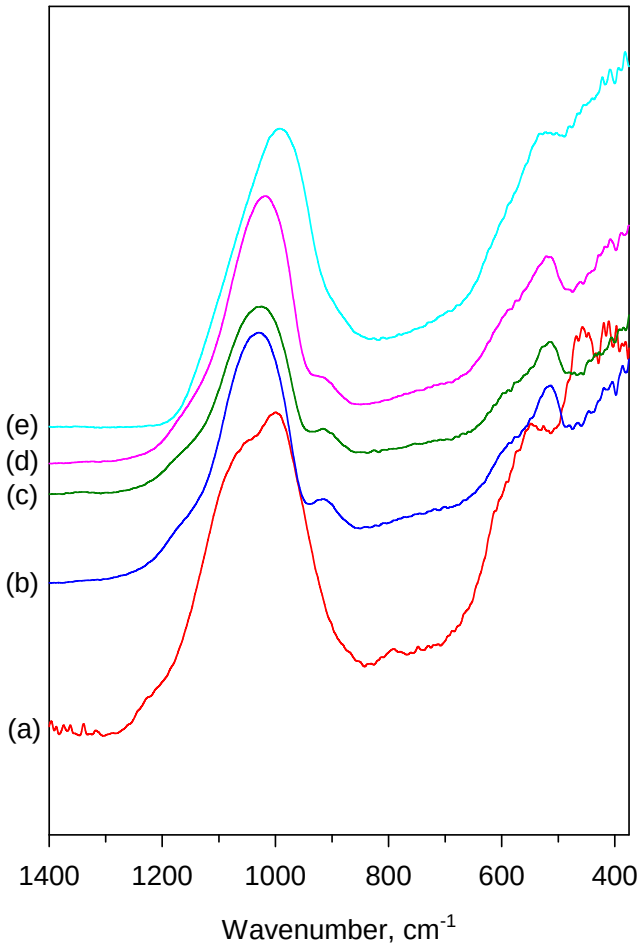

Figure 3.3. FTIR Spectra of Simulants Prepared by Mixing $Fe(NO_3)_3$ With Na_3PO_4 Solutions at Different Initial pH: a) Actual $BiPO_4$ Sludge Tank Waste (Lumetta et al. 2009b), b) pH 7, c) pH 9, d) pH 11, and e) pH 12.3

There was no discernable trend observed in the FTIR spectra of the iron(III) phosphate simulants prepared at different starting Fe concentrations (Figure 3.4). The ν_3(P=O) band varies from 1002 to 1015 cm^{-1}, but these changes do not appear to correlate with the initial Fe concentration. The simulant obtained by adding 0.5 M Fe to 0.5 M Na_3PO_4 appeared to best resemble the actual waste from this particular series of simulants. However, there is not a major difference between this and the simulants prepared at other Fe concentrations.

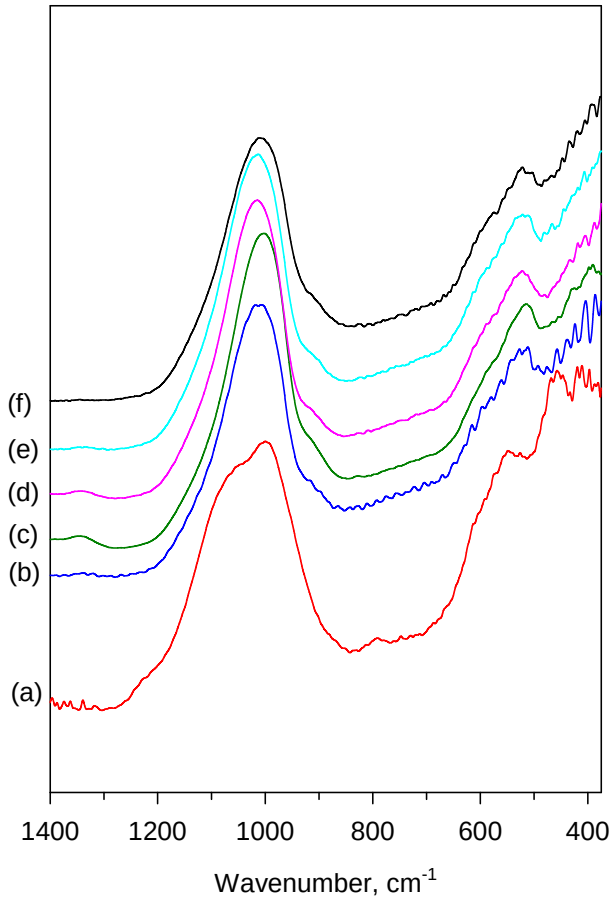

Figure 3.4. FTIR Spectra of Simulants Prepared by Mixing $Fe(NO_3)_3$ With Na_3PO_4 Solutions at Different Initial Concentrations of Fe: a) Actual $BiPO_4$ Sludge Tank Waste (Lumetta et al. 2009b), b) 1 M Fe, c) 0.5 M Fe, d) 0.2 M Fe, e) 0.1 M Fe, and f) 0.02 M Fe

Adding Bi^{3+} to the Fe^{3+} solution used to make the $BiPO_4$ sludge simulant results in a significant deviation from the actual waste material (Figure 3.5). The ν_3(P=O) band shifts from 1013 cm^{-1} to 969 cm^{-1}. Based on this shift, it was concluded that this formulation is not suitable as a simulant for the $BiPO_4$ sludge solids.

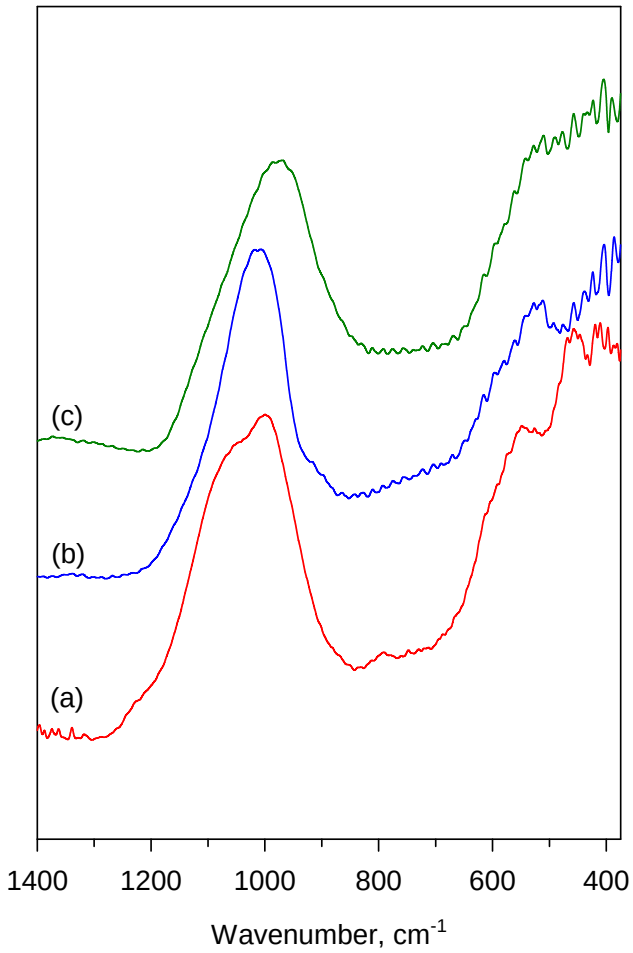

Figure 3.5. FTIR Spectra of Simulants Prepared by Mixing $Fe(NO_3)_3$ and Na_3PO_4 Solutions With and Without Bi^{3+} Present: a) Actual $BiPO_4$ Sludge Tank Waste (Lumetta et al. 2009b), b) Without Bi, and c) With Bi

Figure 3.6 presents the FTIR spectra of simulant phases prepared by adding 1 M $Fe(NO_3)_3$ to a pH 12.3 Na_3PO_4 solution at different temperatures. The FTIR spectra indicate there are no significant differences between the solids formed at different temperatures. The ν_3(P=O) band ranges from 993 to 997 cm^{-1} for these solid phases. This agrees with the results shown in Figure 3.2, which also indicate essentially no temperature-dependence (in the range 25 to 80°C) on the iron(III) phosphate solids formed.

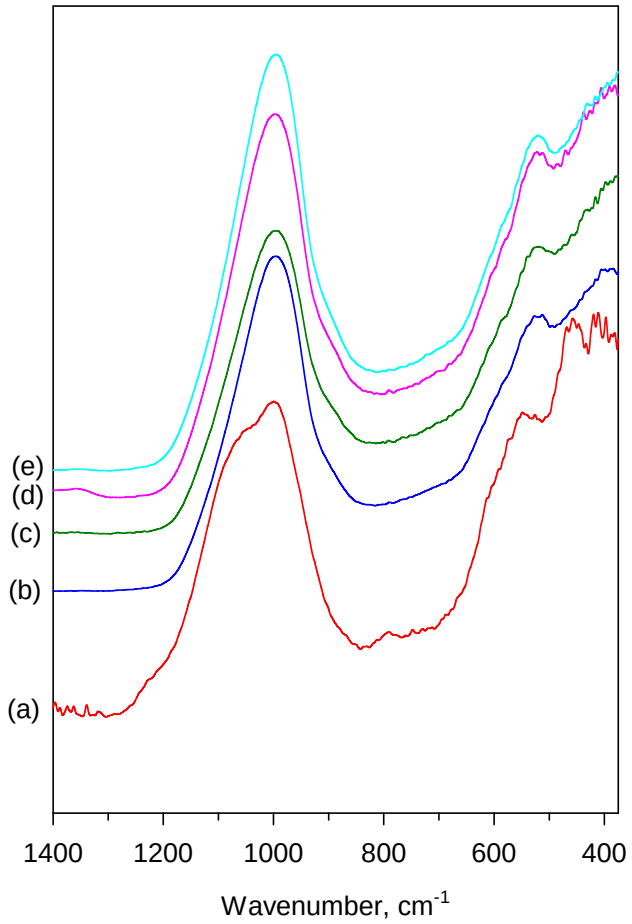

Figure 3.6. FTIR Spectra of Simulants Prepared by Mixing Aqueous $Fe(NO_3)_3$ With Aqueous Na_3PO_4 Adjusted to pH 12.3 at Different Temperatures: a) Actual $BiPO_4$ Sludge Tank Waste (Lumetta et al. 2009b), b) 25°C, c) 40°C, d) 60°C, and e) 80°C

3.1.3 Scale-up of Iron(III) Phosphate Simulant

Based on the results discussed above, the iron(III) phosphate simulant preparation at pH 12 was performed at a larger scale. Figure 3.7 compares the FTIR spectrum of the actual $BiPO_4$ sludge solids with that for the product obtained from the scale-up simulant preparation. The FTIR spectrum of the simulant agrees fairly well with that of the actual waste. Interestingly, the ν_3(P=O) band in the spectrum of the product from the 30-g batch (1009 cm^{-1}) is shifted 14 cm^{-1} to higher energy from the product obtained under analogous conditions at a smaller scale (995 cm^{-1}; Figure 3.6b), indicating that the position of this band is very sensitive to the specific conditions under which the iron(III) phosphate is precipitated. Elemental analysis of the product by ICP-AES indicated 25.6 wt% Fe, 13.2 wt% P, and 1.3 wt% Na. The molar ratio of Fe to P is essentially 1:1, suggesting that the material can best be formulated as $FePO_4 \cdot \times H_2O$. The amount of Na present is relatively minor, with the Na/P molar ratio being 0.13. Thermogravimetric analysis (TGA) indicated the release of water from ambient temperature to approximately 200°C with the maximum release of water at 71°C. The TGA indicated that the $BiPO_4$ sludge simulant was 29.0 wt% water, which is best fit by the empirical formula $FePO_4 \cdot 3.4H_2O$.

Scanning electron microscopy (SEM) examination of the product obtained after grinding and passing through a 0.45-µm sieve revealed the material to consist of agglomerates of submicron particles (Figure 3.8, right). This morphology is consistent with that observed for actual $BiPO_4$ sludge solids (Figure 3.8, left), although the actual waste sample displayed a number of other types of solid particles, which is consistent with the greater complexity of the actual waste material compared to the simulant (Lumetta et al. 2009a). The particle-size distribution (PSD) of the simulant was similar to that seen for the actual waste, but on average, the particles were somewhat smaller in the actual waste material (Table 3.1).

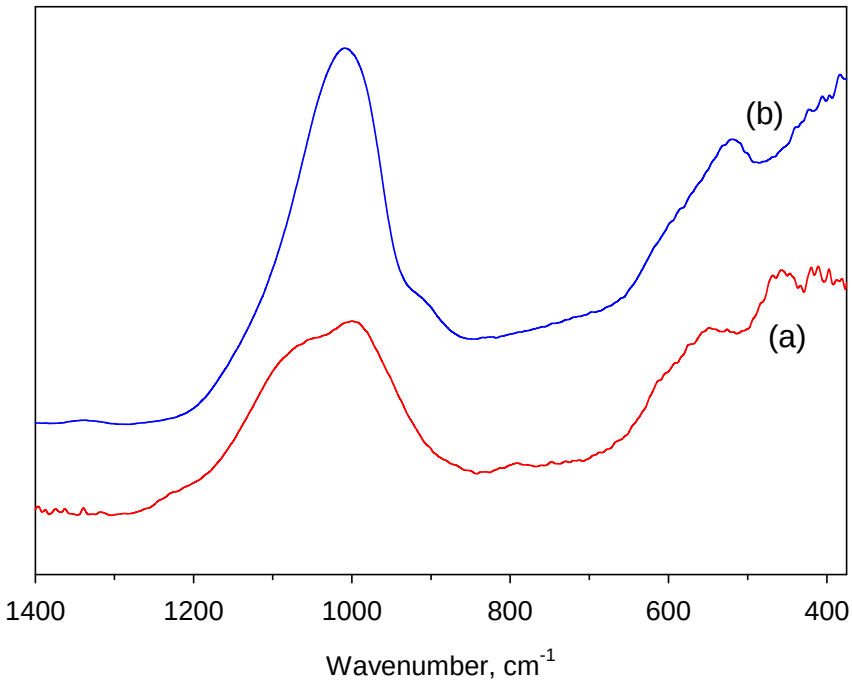

Figure 3.7. FTIR Spectra of Scaled-Up Iron(III) Phosphate Simulant Prepared by Mixing Aqueous $Fe(NO_3)_3$ With Aqueous Na_3PO_4 Adjusted to pH 12.5: a) Actual $BiPO_4$ Sludge Tank Waste (Lumetta et al. 2009b) and b) Scaled-Up Simulant

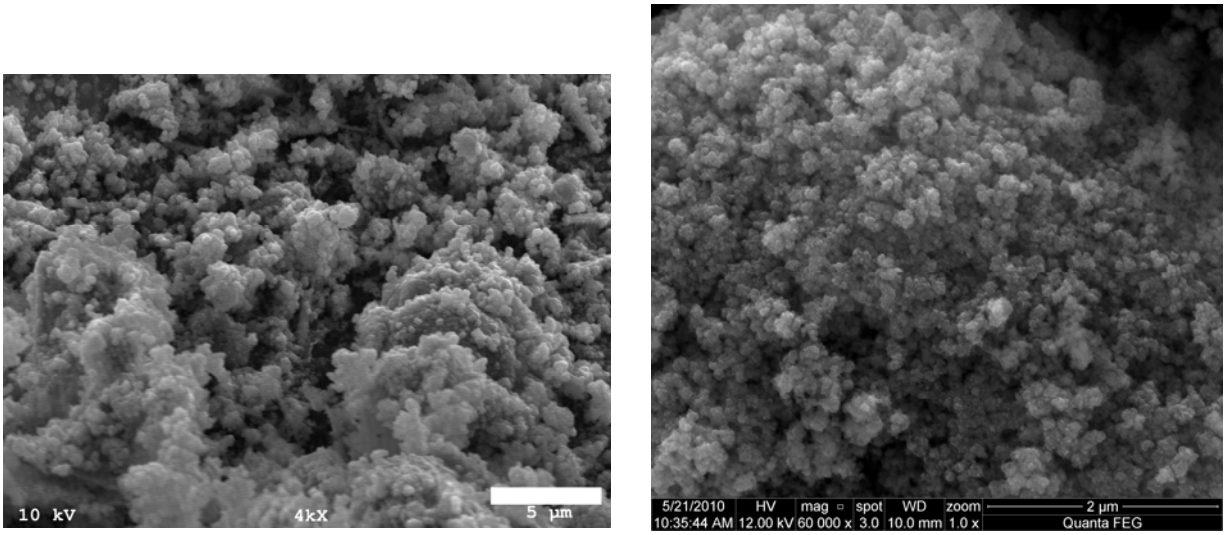

Figure 3.8. SEM Micrographs of Scaled-Up Iron(III) Phosphate Simulant Prepared by Mixing Aqueous $Fe(NO_3)_3$ With Aqueous Na_3PO_4 Adjusted to pH 12.5; Left) Actual $BiPO_4$ Sludge Tank Waste (Lumetta et al. 2009a), Right) Scaled-Up Simulant

Table 3.1. Comparison of PSDs (volume basis) for the $BiPO_4$ Sludge Simulant and Actual $BiPO_4$ Sludge (data taken from Lumetta et al. 2009a)[(a)]

	Actual Waste	Simulant
d(10)	1.2	3.1
d(50)	6.9	18
d(90)	31	49

(a) The d(10), d(50), and d(90) values represent the cumulative diameters (in µm) corresponding to the 10^{th}, 50^{th}, and 90^{th} volume percentiles, respectively.

3.2 Parametric Leaching

3.2.1 Variable NaOH Concentration at Ambient Temperature

An initial screening test was conducted in which the $BiPO_4$ simulant was treated with 0.5, 1.0, and 2.0 M NaOH at ambient temperature. The progress of the reaction was qualitatively monitored by Raman spectroscopy using the phosphate band at 938 cm^{-1}. The Raman results suggested that the reaction occurred rapidly at all three NaOH concentrations with little noticeable difference from the spectra at 15 min and at 175 min, although the signal intensity was quite weak, so this can only be considered to be a qualitative observation. The degree of P removal in each case was determined from the amount of P found in the composite leaching and washing solution (the measured P concentration times the volume of solution). This was divided by the amount of P contained in the sludge sample used (0.132 g P/g simulant). The results were as follows:

[NaOH], M	*OH^-/P Molar Ratio*	*P Removed, %*
0.5	13	85
1.0	23	76
2.0	43	87

The amount of P removed at 0.5 M NaOH was essentially the same as that removed at 2.0 M NaOH. The reason for the slightly lower removal observed for 1.0 M NaOH is not clear, but regardless, there does not appear to be any advantage in using higher NaOH concentrations.

Elemental analysis of the solids after leaching indicated 52, 53, and 55 wt% Fe for the products from leaching at 0.5, 1.0, and 2.0 M NaOH, respectively. These values are consistent with the formation of $Fe(OH)_3$ (52.3 wt% Fe). Very little Na (2 wt%) or P (0.1 to 0.3 wt%) remained in the solids after leaching.

3.2.2 Variable Temperature at Constant 0.5 M NaOH

Temperature had little effect on the leaching of phosphate from the $BiPO_4$ simulant, with the results obtained at 25°C being very similar to those obtained at 60°C. The amount of P removed from the $BiPO_4$ simulant solids was 98.7, 97.0, and 98.2% after leaching with 0.5 M NaOH at 25, 40, and 60°C, respectively. In all cases, the leaching time was 15 min, so the metathesis from $FePO_4$ to Na_3PO_4 is relatively rapid, even at 25°C. Analysis of the residual solids indicated 58, 52, and 65 wt% Fe from the tests at 25, 40, and 60°C, respectively. These values are consistent with the formation of $Fe(OH)_3$ (52.3 wt% Fe) along with dehydrated forms such as FeOOH (63 wt% Fe) and/or Fe_2O_3 (69.9 wt% Fe).

3.3 Phosphate Removal by Treatment with Lime

3.3.1 First Kinetic Test at Ambient Temperature

Figure 3.9 shows the Na and P concentrations as a function of time during treatment of a 0.19 M Na_3PO_4/1 M NaOH solution with CaO at ambient temperature. Surprisingly, there was an ~9% decrease in the Na concentration during the first 5 min of reaction, but no subsequent decrease in the Na concentration was observed out to 120 min. The P concentration declined steadily, especially over the first 60 min of reaction. The rate of decrease in the P concentration leveled off after 60 min, but the P concentration still declined between 90 and 120 min. A total of 77% of the P was removed from the 0.15 M Na_3PO_4/1 M NaOH solution during this experiment.

The liquid phase was titrated with standard HCl both before and after treatment with CaO to determine the amount of free hydroxide released per mole of phosphate precipitated. The starting solution displayed two equivalence points. The first one was taken to be associated with free hydroxide ion, while the second one was taken to be associated with protonation of the phosphate (or hydrogen phosphate) ion. In this way, the initial free hydroxide concentration was determined to be 0.98 M, while the initial phosphate concentration was determined to be 0.20 M. The latter value is in excellent agreement with the P concentration of 0.19 M determined by ICP-OES. The former value is consistent with the target value of 1.0 M NaOH in the starting solution. Thus, the interpretation of the two equivalent points in the titration curve appears reasonable.

Following the treatment with CaO, the second equivalence point could be clearly distinguished for only one of the triplicate titration runs. Based on this particular titration, the phosphate concentration after CaO treatment was determined to be 0.08 M. This is reasonably consistent with the value of 0.04 M determined by ICP-OES, given the large experimental uncertainty associated with the titration measurement. The free hydroxide concentration after the CaO treatment was 1.13 M, an increase of 0.15 M OH^- over the initial concentration of 0.98 M. In comparison, the decrease in the phosphate concentration for this experiment was 0.19 – 0.04 = 0.15 M. Therefore, one equivalent of hydroxide ion was released into solution for every equivalent of phosphate removed. It should be noted that the amount of hydroxide ion released per mole of phosphate precipitated is considerably less than the 3 moles OH^-/mole PO_4^{3-} expected base on Eq. 1.1. So, it seems unlikely the solid product is solely hydroxyapatite.

Figure 3.10 shows the FTIR and Raman spectra of the solid product collected after treating the 0.19 M Na_3PO_4/1 M NaOH solution with CaO. Both the FTIR and Raman spectra suggest the presence of hydroxyapatite in the solids collected after the CaO treatment. However, both also indicate the presence of at least one other solid phase. The phosphate stretching vibrations in this unidentified phase(s) are shifted to significantly higher energy in the FTIR spectrum (1413 and 1460 cm^{-1}). As discussed in Section 3.5, these bands might be caused by the presence of calcium carbonate. X-ray diffraction (XRD) analysis of the solids also supports the presence of hydroxyapatite, but the diffraction peaks are quite broad, indicating that it is not highly crystalline (Figure 3.11). There is also a sharp diffraction peak at 29.44 2θ that is consistent with brushite, $CaHPO_4 \cdot 2H_2O$, but this could not be confirmed because other peaks from this species could not be definitively distinguished from the background. Also, there was no evidence for $CaHPO_4 \cdot 2H_2O$ in the FTIR spectrum.

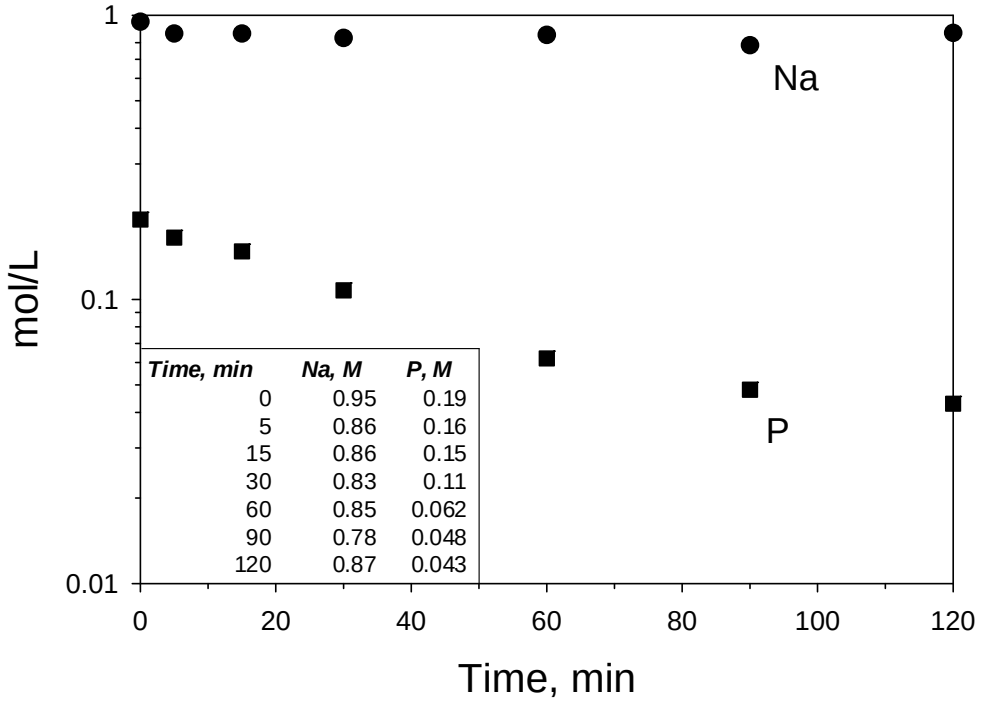

Figure 3.9. Sodium and Phosphorus Concentrations as a Function of Time During the First Phosphate Precipitation Test at Ambient Temperature

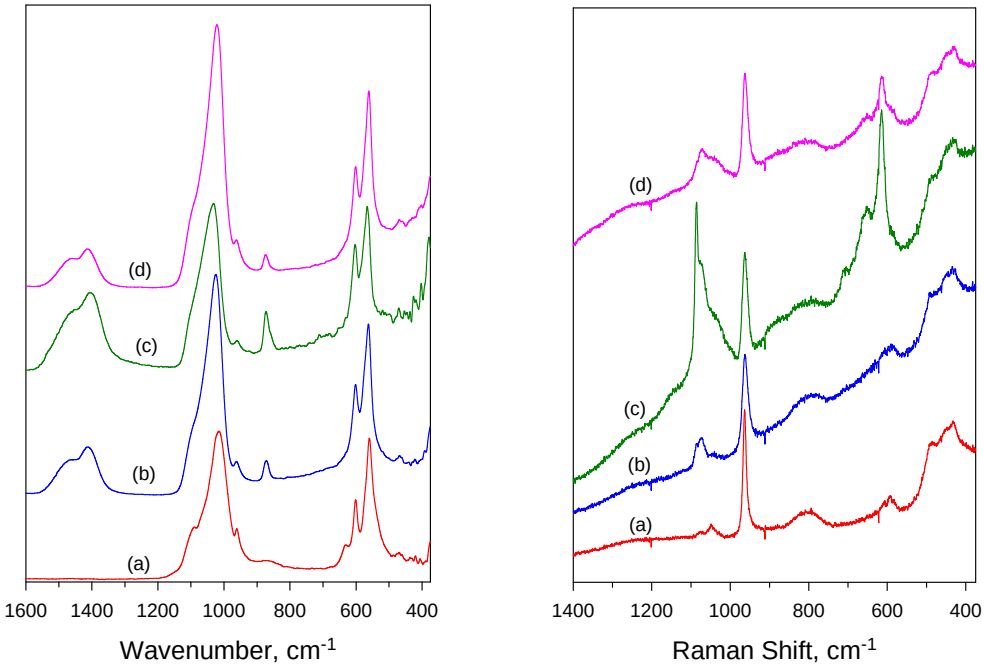

Figure 3.10. FTIR (left) and Raman (right) Spectra of Solid Residuals Remaining After Treatment of Na_3PO_4/1 M NaOH Solutions With CaO: a) Hydroxyapatite, b) Solid Product from First Test at Ambient Temperature, c) Solid Product from Test at Ambient Temperature With Increased Amount of CaO, and d) Solid Product from Test at 40°C

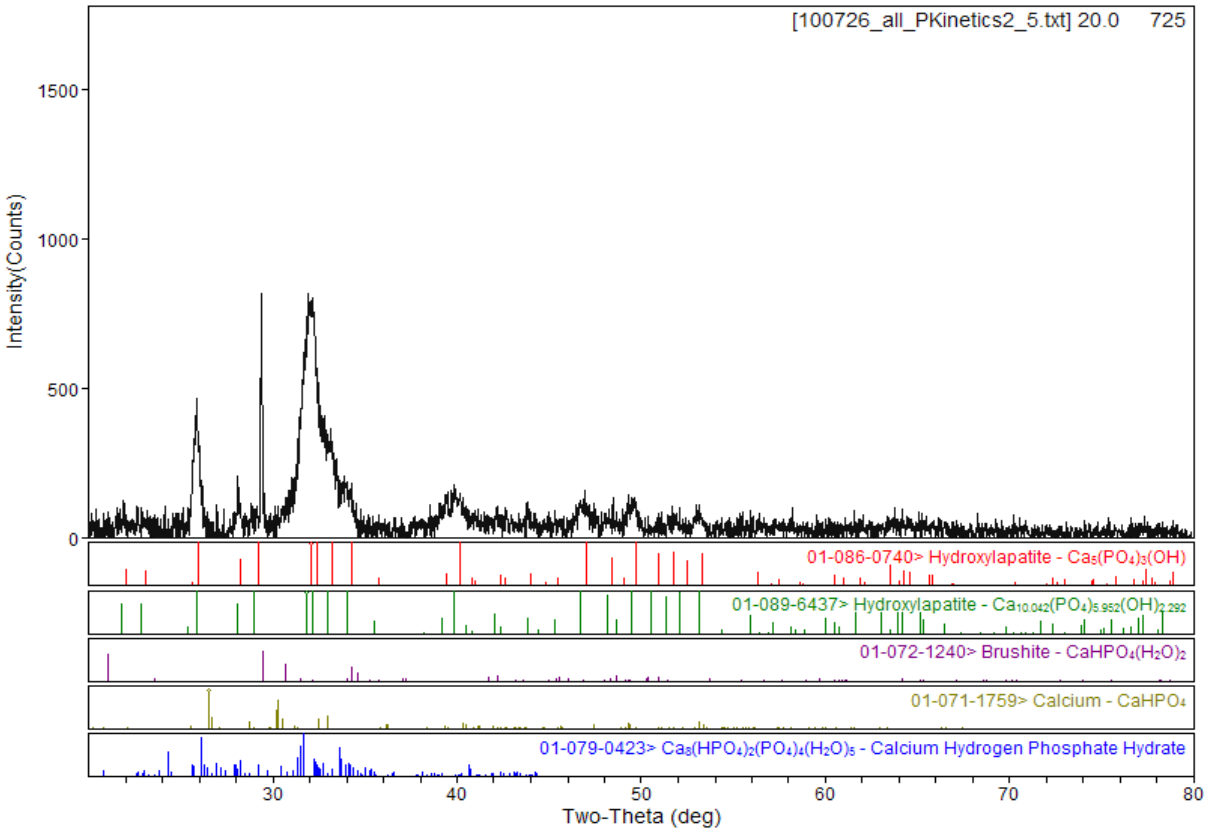

Figure 3.11. XRD Pattern for the Solid Remaining After Treating 0.19 M Na_3PO_4/1 M NaOH Solutions With CaO at Ambient Temperature (1.8 mole Ca/mol P)

3.3.2 Kinetic Test at 40°C

Figure 3.12 shows the Na and P concentrations as a function of time during treatment of a 0.18 M Na_3PO_4/1 M NaOH solution with CaO at ambient temperature. In this case, the Na concentration remained essentially constant throughout the course of the experiment. As was the case at room temperature, the P concentration declined steadily, but was nearly constant after the first 60 min of reaction. Only 68% of the P was removed from the 0.18 M Na_3PO_4/1 M NaOH solution at 40°C, suggesting that elevating the temperature has an adverse effect on phosphate removal.

The initial and final liquid phases were titrated with standard HCl to determine the amount of free hydroxide released per mole of phosphate precipitated. The initial free hydroxide concentration was determined to be 1.23 M, while the initial phosphate concentration was determined to be 0.21 M (compared to 0.18 M determined by ICP-OES). Following the treatment with CaO, the free hydroxide concentration was 1.35 M, and the phosphate concentration, as determined by titration, was 0.07 M (compared to 0.06 M determined by ICP-OES). So in this case, a 0.12 M increase in the free hydroxide occurred upon treatment with CaO. The decrease in the phosphate concentration for this experiment was 0.18 – 0.06 = 0.12 M. Again, one equivalent of hydroxide ion was released into solution for every equivalent of phosphate removed, which is less than that expected from Eq. 1.1.

Figure 3.10 shows the FTIR and Raman spectra of the solid product collected after treating the 0.18 M Na_3PO_4/1 M NaOH solution with CaO at 40°C. The spectral features of the solid product obtained in this experiment closely resemble those for the product obtained at ambient temperature. Again, both the FTIR and Raman spectra suggest the presence of hydroxyapatite in the solid product, along with another species. XRD analysis of the solids obtained after CaO treatment at 40°C also supports the presence of hydroxyapatite with a diffraction pattern similar to that observed for the product obtained at ambient temperature.

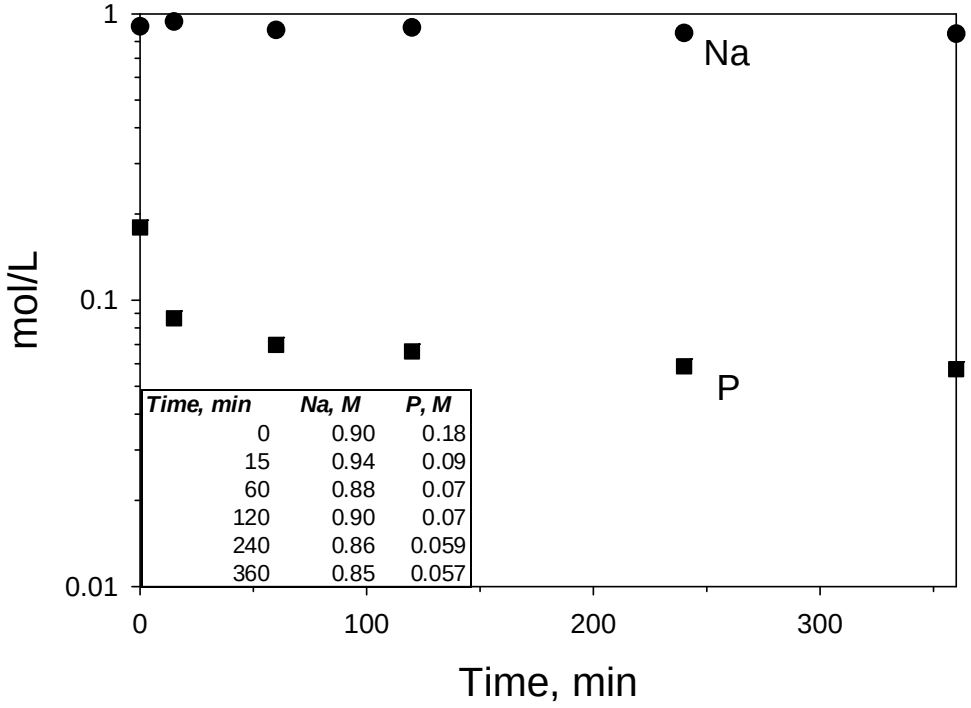

Figure 3.12. Sodium and Phosphorus Concentrations as a Function of Time During the Phosphate Precipitation Test at 40°C

3.3.3 Second Kinetic Test at Ambient Temperature

Because only ~70 to 75% of the phosphate was removed from the Na_3PO_4/NaOH solution in the two experiments described above, it was of interest to determine if increasing the amount of CaO would improve the phosphate removal. In this experiment, the amount of CaO used was doubled to 4 mole Ca/mole PO_4^{3-}. Figure 3.13 shows the Na and P concentrations as a function of time during treatment of 10 mL 0.18 M Na_3PO_4/1 M NaOH solution with 0.4 g CaO at ambient temperature. In this case, essentially quantitative (> 99%) removal of phosphate was achieved. One potential explanation for the incomplete removal of phosphate in the first test could be that the calcium oxide used is not 100% CaO. For example, the presence of $Ca(OH)_2$ would lower the effective molar concentration of Ca. The FTIR spectrum of the calcium oxide used showed a sharp peak at 3639 cm^{-1}, which might support the presence of some calcium hydroxide.

The initial free hydroxide concentration was determined to be 1.08 M and the phosphate concentration 0.25 M by titration with standard HCl. The latter value is considerably higher than that

obtained by ICP-OES (0.18 M). After treatment with CaO, the free hydroxide concentration increased to 1.42 M. Surprisingly, the moles of hydroxide released in this test per mole of phosphate precipitated was approximately 2, which is double that obtained in the previous tests, but again below that expected for the reaction shown in Eq. 1.1. Perhaps this simply reflects the dissolution of CaO as calcium hydroxide. Consistent with ICP-OES observation of quantitative phosphate removal, only a single equivalence point was observed in the titration of the solution after the CaO treatment.

Figure 3.10 shows the FTIR and Raman spectra of the solid product collected after treating the 0.18 M Na_3PO_4/1 M NaOH solution with an increased amount of CaO at ambient temperature. Although the FTIR and Raman spectra of this product again suggest the presence of hydroxyapatite, the relative proportion of the other solid species appears to be greater in this solid product.

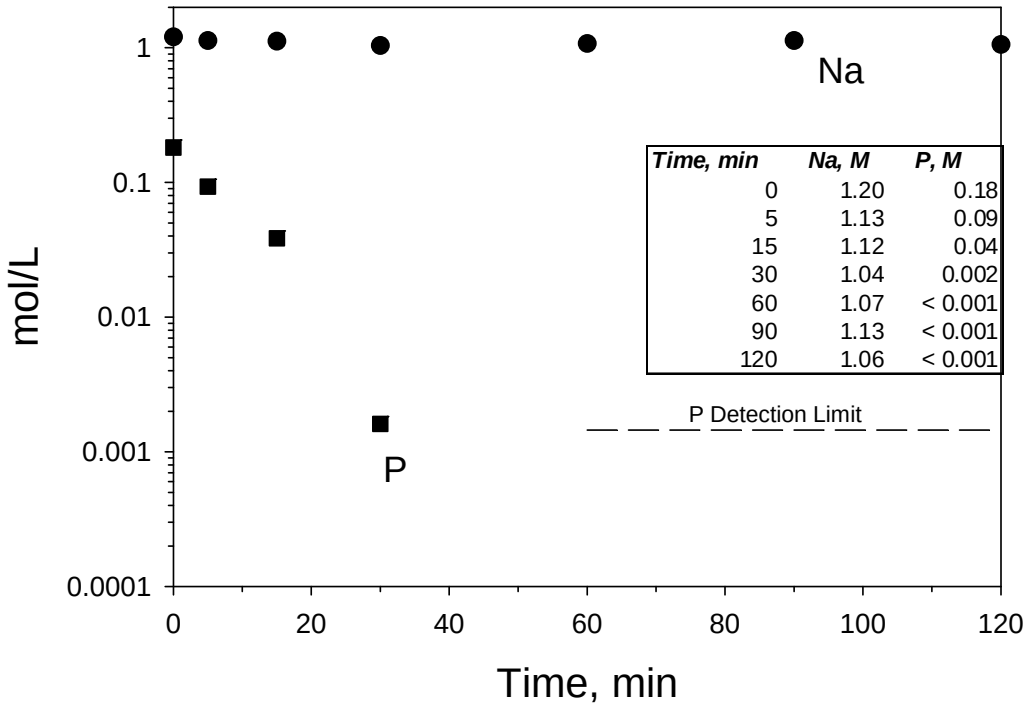

Figure 3.13. Sodium and Phosphorus Concentrations as a Function of Time During the Second Phosphate Precipitation Test at Ambient Temperature

3.4 Phosphate Solubility Modeling

This section describes the thermodynamic modeling activities that were performed to support the development of the process for removing phosphate from the bismuth phosphate sludge HLW. The thermodynamic modeling activities consisted of three specific tasks: 1) a detailed comparison of the thermodynamic model predictions with existing experimental data for important electrolyte components of the bismuth phosphate wastes, 2) model application studies using past and current leaching data, and 3) an update of the thermodynamic database to improve the model predictions. Each of these tasks is described in detail below. The thermodynamic model used in this study is the Environmental Simulation Program (ESP; OLI, Inc., Morris Plains, NJ) with the newest mixed-solvent electrolyte (MSE) database.

3.4.1 Model Comparison Studies

One of the key objectives of the thermodynamic modeling task is to predict the dissolution behavior of key components in the bismuth phosphate tank waste during leaching with aqueous NaOH. Adding NaOH into tank waste results in an aqueous or supernatant solution that contains NaOH, the phosphate released from the waste, and other electrolyte ions that can dissolve from the waste. The release of phosphate from the waste can be limited by the precipitation of insoluble sodium phosphate species, including $Na_3PO_4 \cdot 8H_2O$ and $Na_3PO_4 \cdot 1/4NaOH \cdot 12H_2O$, or by co-precipitation with other anions, especially fluoride (e.g., $Na_7F(PO_4)_2 \cdot 19H_2O$). The solubility of all of these compounds also depends upon the concentrations of the other electrolyte ions that are released from the waste upon contact with the NaOH solution. The major electrolyte ions that can dissolve from the waste include nitrate, nitrite, sulfate, carbonate, and fluoride. Because of this possible variability in the chemical composition of the leachate solutions, it was decided to test the thermodynamic model predictions of phosphate solubility in a wide variety of electrolyte solutions within the more general $Na\text{-}OH\text{-}NO_3\text{-}NO_2\text{-}SO_4\text{-}CO_3\text{-}F\text{-}PO_4\text{-}H_2O$ system as a function of temperature.

Since fluoride-containing phases are predicted to be important in the bismuth phosphate sludge and salt cake supernatant (see Section 3.4.2) and can influence phosphate solubility through formation of the $Na_7F(PO_4)_2 \cdot 19H_2O$ phase, it was also important to compare the predictions of fluoride solubility in similar electrolyte solutions. This was the same procedure used by Felmy and MacLean (2001) in developing and testing the Pitzer thermodynamic model for similar solutions. Table 3.2 lists all of the chemical systems analyzed in this model comparison study. All of the available solubility data in these chemical systems were then obtained and converted to units of molality for direct comparison with the thermodynamic model predictions. The exact comparisons between model and experiment are shown in Figure 3.14 through Figure 3.16.

Table 3.2. Summary of the Common-Ion Ternary Systems in the $Na\text{-}OH\text{-}NO_3\text{-}NO_2\text{-}SO_4\text{-}CO_3\text{-}F\text{-}PO_4\text{-}H_2O$ System for Which Model Comparison Studies Were Conducted

NaF Containing Systems	Na_3PO_4 Containing Systems
NaF-NaOH	Na_3PO_4-NaOH
NaF-$NaNO_3$	Na_3PO_4-$NaNO_3$
NaF- Na_2SO_4	Na_3PO_4-Na_2CO_3
NaF – Na_2CO_3	Na_3PO_4-Na_2SO_4
NaF – Na_3PO_4	Na_3PO_4-$NaNO_2$

Comparisons of the solubility relations in the sodium fluoride systems (Figure 3.14) are very good for the NaOH-containing solutions (Figure 3.14a), $NaNO_3$ solutions (Figure 3.14b,c), and even for the Na_2SO_4-containing systems where the double salt $NaF \cdot Na_2SO_4$ forms at around 0.8 M Na_2SO_4 (Figure 3.14d). The predictions are also reasonably good for the Na_2CO_3 solutions up to approximately 1 M Na_2CO_3. Above 1 M Na_2CO_3, the model predictions are too high by as much as a factor of two (Figure 3.14e). Given the expected concentrations of Na_2CO_3 in the leachate solutions, these very high Na_2CO_3 solutions are unlikely to occur during processing of bismuth phosphate sludge, so the model predictions should be satisfactory for this system.

Comparisons of the solubility relations in the sodium phosphate systems (Figure 3.15) show good agreement with the experimental data in $NaNO_3$ solutions (Figure 3.15b,c,d) and in sodium carbonate solutions (Figure 3.15f). The agreement between model and experiment is also very good for the mixed Na_3PO_4-NaOH solutions at 25°C, but then appears to be about a factor of two low at higher temperature (50°C) (Figure 3.15a). Interestingly, the predictions for the higher order Na_3PO_4-NaOH-$NaNO_3$ system are actually very good after adding $NaNO_3$ to the pure NaOH solutions (Figure 3.15d,e), even at a higher temperature. The reason for the discrepancy in the absence of $NaNO_3$ at 50°C is unclear, but may have to do with the transition in phase stability from $Na_3PO_4 \cdot 1/4NaOH \cdot 12H_2O$ at lower temperature to $Na_3PO_4 \cdot 8H_2O$ at higher temperature. The model also apparently over-predicts the solubilities in Na_2SO_4-containing solutions. However, as previously discussed by Felmy and MacLean (2001), the experimental solubility data in this system appear to be inconsistent when compared with other 2:1 electrolytes (i.e., Na_2CO_3) (Figure 3.15g). The most serious discrepancy between model and experiment occurs in solutions containing $NaNO_2$. The model over-predicts the phosphate solubility by orders of magnitude at high $NaNO_2$ (Figure 3.15h). This appears also to be related to the transition from the stable $Na_3PO_4 \cdot 1/4NaOH \cdot 12H_2O$ at lower $NaNO_2$ concentration (higher water activity) to $Na_3PO_4 \cdot 8H_2O$ at higher concentration. Hence as part of this project, we elected to improve the thermodynamic model for this system as described in a later section.

Finally, the model predictions in the mixed NaF-Na_3PO_4 system (Figure 3.16) agree very well with all of the existing experimental data.

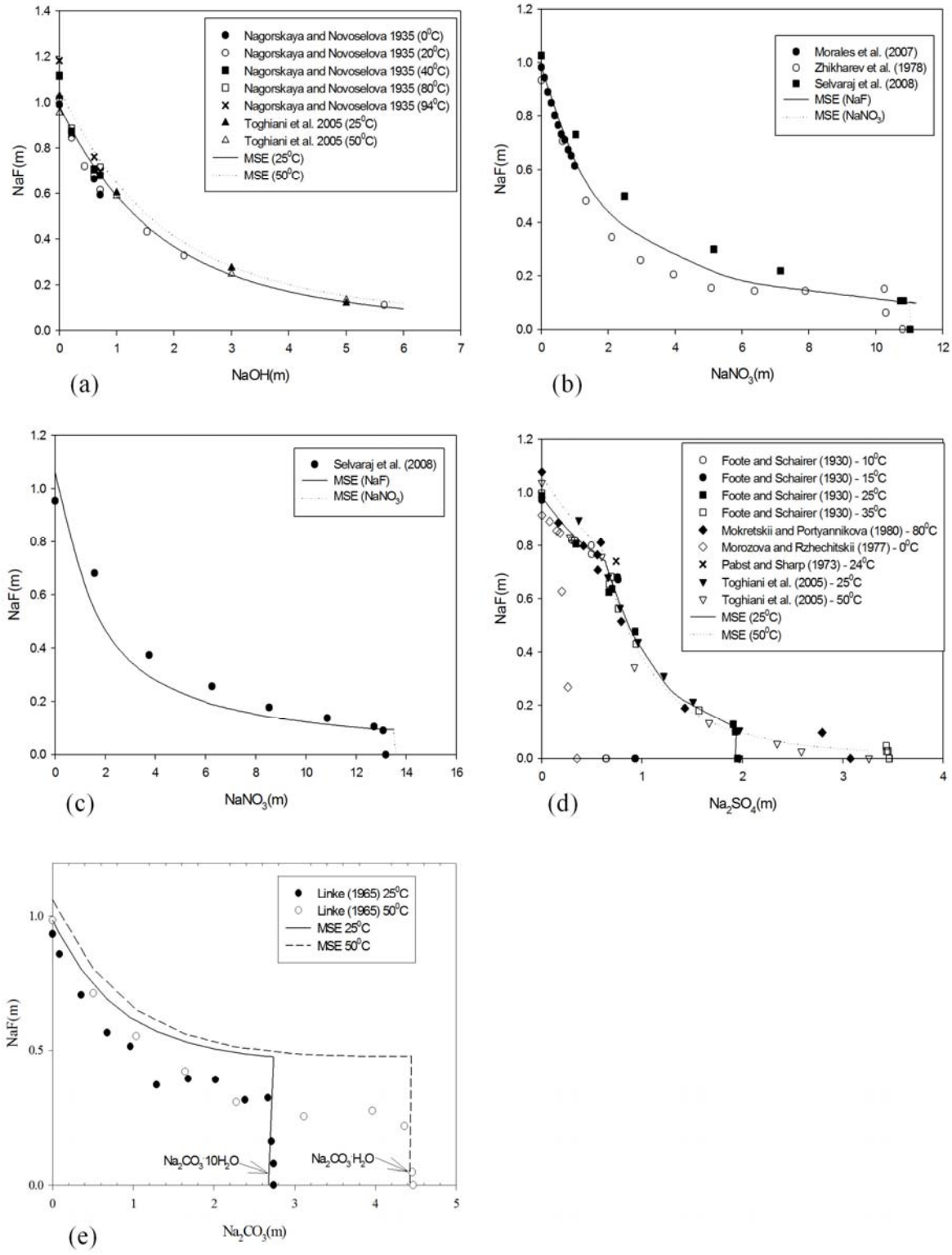

Figure 3.14. Experimental Data and MSE Simulations of Solubility Relations in NaF Containing Systems: a) NaF-NaOH-H_2O at Different Temperatures, b) NaF-$NaNO_3$-H_2O (25°C), c) NaF-$NaNO_3$-H_2O (50°C), d) NaF-Na_2SO_4-H_2O at Different Temperatures, and e) NaF-Na_2CO_3-H_2O at 25°C and 50°C

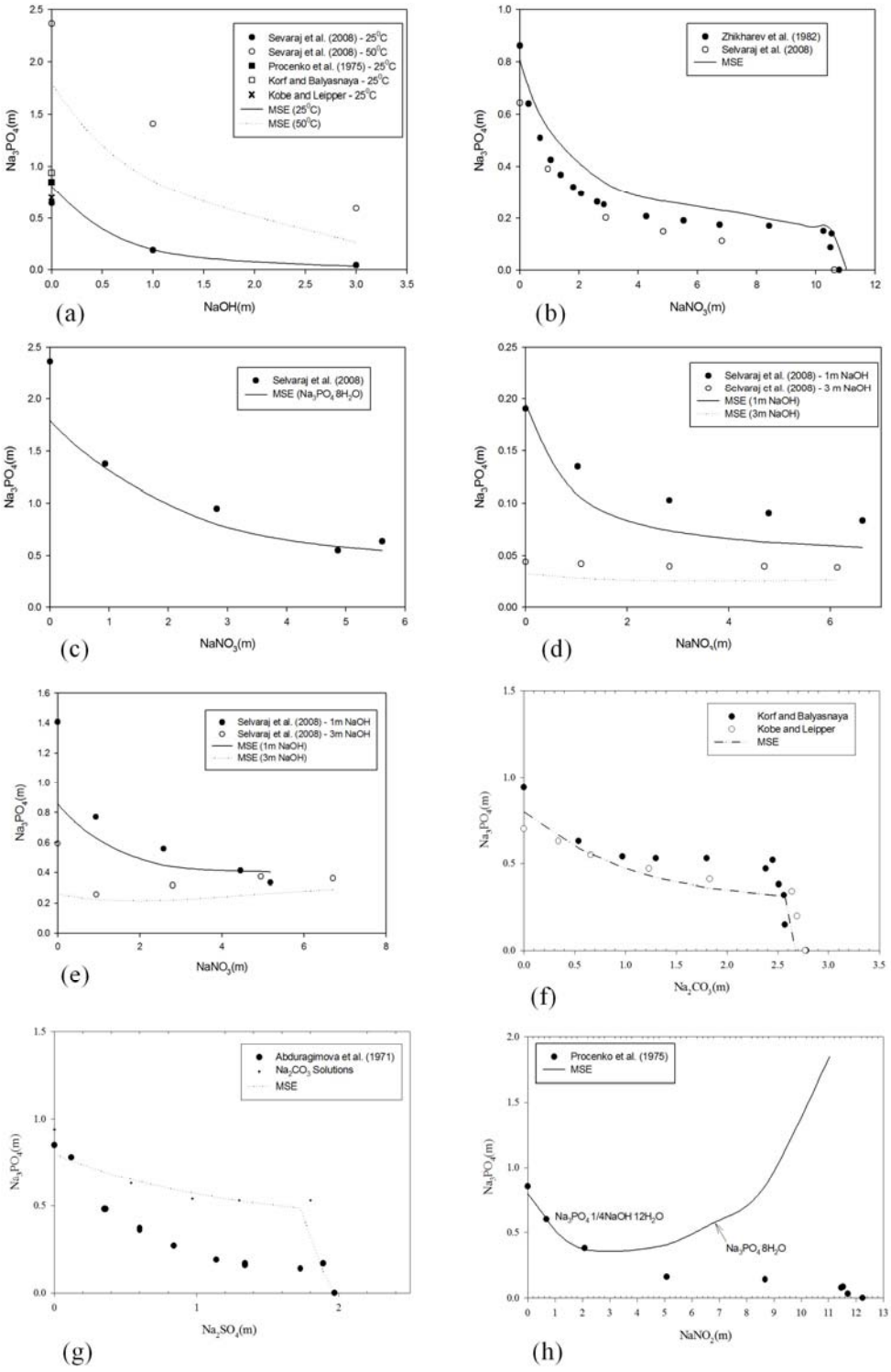

Figure 3.15. Experimental Data and MSE Simulations of the Solubility Relations in Na_3PO_4 Containing Systems: a) Na_3PO_4-NaOH-H_2O at 25˚C and 50˚C, b) Na_3PO_4-$NaNO_3$-H_2O 25˚C, c) Na_3PO_4-$NaNO_3$-H_2O 50˚C, d) Na_3PO_4-$NaNO_3$-NaOH-H_2O 25˚C, e) Na_3PO_4-$NaNO_3$-NaOH-H_2O 25˚C, f) Na_3PO_4-Na_2CO_3-H_2O 25˚C, g) Na_3PO_4-Na_2SO_4-H_2O 25˚C, and h) Na_3PO_4-$NaNO_2$-H_2O 25˚C

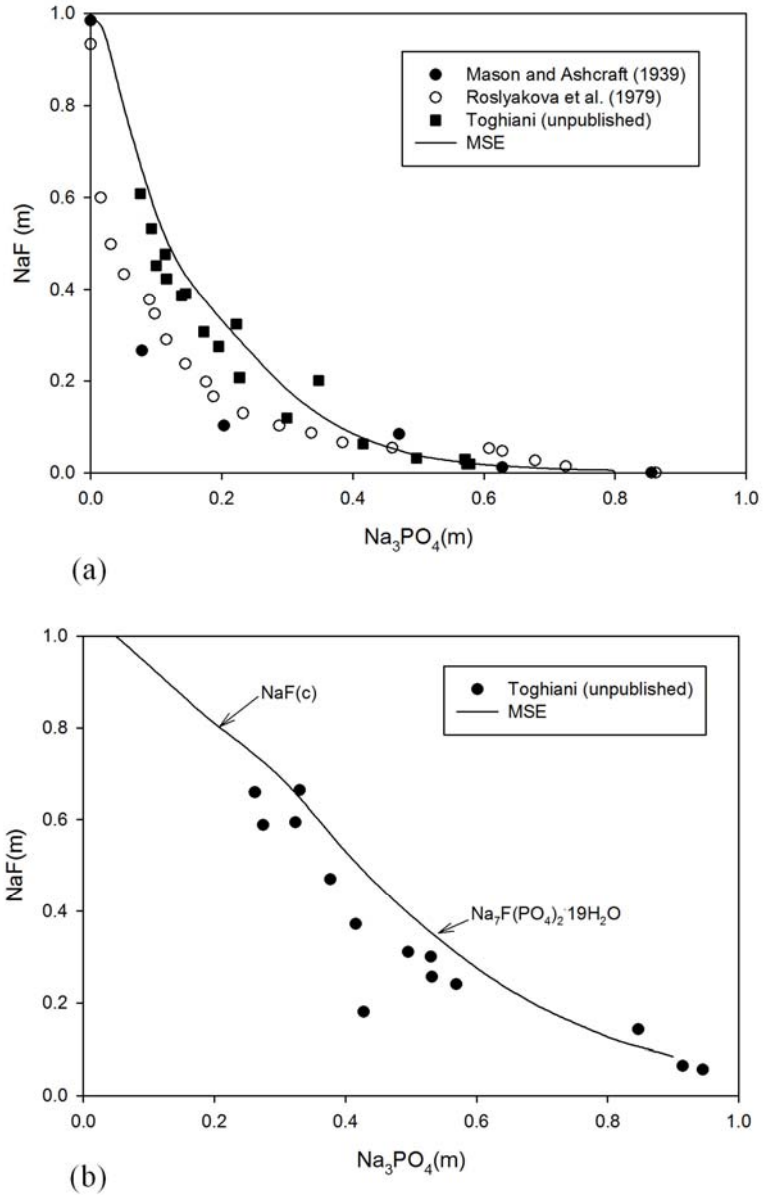

Figure 3.16. Experimental Data and MSE Simulations of the Solubility Relations in the Na_3PO_4-NaF-H_2O System at a) 25°C and b) 50°C

3.4.2 Model Applications

In this section, the ESP model with the database that was tested in simple electrolyte systems was used to analyze the complex waste solutions resulting from the leaching of actual samples of bismuth phosphate sludge and bismuth phosphate saltcake. Results of the model simulations of the tests performed with that actual waste (Lumetta et al. 2009a) are described below.

3.4.2.1 Analysis of Leaching Studies (FY-09 results)

In this section, results from supernatant analysis and caustic leaching of bismuth phosphate sludge (Group 1 Test Material), bismuth phosphate saltcake (Group 2 Test Material), and composite waste (Group 1/2 Test Material) were analyzed using the thermodynamic model to predict the formation of possible phosphate-solubility limiting phases and propose possible methods for maximizing the efficiency of the overall leaching process.

3.4.2.1.1 Group 1 Test Material—Bismuth Phosphate Sludge

Lumetta et al. (2009a) report the analysis of bismuth phosphate sludge supernatant, washed solids, and caustic leached sludge. The analytical data used in these simulations for supernatant and washed solids were taken from Table 3.6 of Lumetta et al. 2009a and those for the leached sludge solids were taken from Appendix G of that report.

Supernatant and Wash Composite

Model simulations using the reported supernatant composition indicated that the supernatant was either in equilibrium or oversaturated with respect to the sodium fluoride-sodium phosphate double salt, $Na_7F(PO_4)\cdot 19H_2O$, indicating that this phase is likely controlling the solubility of fluoride and phosphate in the composite supernatant. This result is not surprising given the relatively low solubility of this phase at lower temperatures (see Figure 3.16a). The other major sodium-containing phases, such as sodium nitrate, sodium nitrite, or the normal sodium phosphate ($Na_3PO_4\cdot ¼NaOH\cdot 12H_2O$), were all below saturation in the supernatant liquid.

It was not possible to confidently assess the solubility-limiting phases for compounds of several other elements, including U, Al, Bi, Zr, Ca, or Fe, because the concentrations of these element were all below the analytical method detection limit. However, if the maximum detection limit values were used in the modeling simulations, the results indicated the formation of uranyl hydroxide [$UO_2(OH)_2$], bismuth oxide (Bi_2O_3), sodium aluminosilicate ($Na_2Al_2Si_3O_{10}\cdot 2H_2O$), zirconium silicate ($ZrSiO_4$), hematite ($Fe_2O_3$), and fluoroapatite [$Ca_5F(PO_4)_3$].

In the case of the composite washing solution, the model predicts that $Na_7F(PO_4)\cdot 19H_2O$ is significantly under-saturated as a result of the decreased sodium and phosphate concentrations in the washing solution. Hence, washing the solids is an important step to remove water-soluble salts from the bismuth phosphate sludge. If the maximum analytical detection limit values are used in the model simulations for the U, Al, Bi, Zr, Ca, or Fe components, the predicted stable phases are the same as in the supernatant solutions described above.

Analysis of the washed solids by XRD, SEM-electron dispersive spectroscopy (EDS), and transmission electron microscopy (TEM) indicated the possible presence of several phases in the washed solids, including sodium nitrate ($NaNO_3$), ammonium aluminum hydrogen phosphate ($NH_4AlHP_3O_{10}$), bismuth phosphate ($BiPO_4$), and vauxite ($FeAl_2(PO_4)_2(OH)_2\cdot 6H_2O$) (see Table 3.11 in Lumetta et al. 2009a). However, many of these phases were labeled as possible or questionable. Only three phases were labeled as either excellent or probable in terms of their probability of occurrence: sodium nitrate, ammonium aluminum hydrogen phosphate, and bismuth phosphate. We were unable to assess the possible formation of ammonium aluminum hydrogen phosphate because of the lack of analytical data on

ammonium. Sodium nitrate is clearly under-saturated in both the bismuth phosphate supernatant and wash solutions. Hence, sodium nitrate must have formed from evaporation of the interstitial liquid during the drying of the solids before analysis. $BiPO_4$ stability was also difficult to determine because neither the pH nor the free hydroxide was determined in the wash solution. However, our modeling predictions of pH (11 to 12) indicated that the most stable bismuth-containing phase is the oxide or hydroxide, not $BiPO_4$. This is consistent with other characterizations of the bismuth phosphate sludge solids (Lumetta et al. 2009b). The possible presence of vauxite is interesting because it is an Fe(II)-containing phase. To simulate possible reducing conditions, the Fe was added into the model as Fe(II) and the Cr as Cr(III). Under such conditions, the stable phases are chromium oxyhydroxide (CrOOH) and chromite ($FeCr_2O_4$). Vauxite is not in the thermodynamic database.

Parametric Leaching Studies

Leaching studies were performed on the Group 1 Test Material at three different temperatures (40, 60, and 80°C) and at two different concentrations of NaOH (1M and 3M) (Lumetta et al. 2009a). At 40°C and 1 M NaOH, the modeling results indicate equilibrium or over-saturation with respect to sodium silicate ($Na_2SiO_3 \cdot 8H_2O$), uranyl hydroxide [$UO_2(OH)_2$], and bismuth oxide (Bi_2O_3). Possible saturation with respect to Bi_2O_3 or $Bi(OH)_3$, which is also close to equilibrium, is an indication that adding base has shifted the equilibrium away from any possible $BiPO_4$ precipitate. Saturation with respect to $Na_2SiO_3 \cdot 8H_2O$ should be considered as uncertain considering the normal highly soluble nature of most sodium silicates. If the formation of this phase is suppressed, the additional silica in solution is still not predicted to result in the formation of sodium aluminosilicates in the MSE database.

The 1 M NaOH/40°C leaching solution is significantly under-saturated with respect to all sodium phosphate phases. Hence, these phases should not place upper limits on the concentration of dissolved phosphate in this solution. The sodium phosphate phase closest to equilibrium was the normal phosphate. However, the phosphate concentration in the leaching solution would need to increase 17 times to reach saturation with respect to this phase. Hence, leaching the Group 1 Test Material at these relatively low concentrations of NaOH should be sufficient to remove the readily soluble phosphate even if the total phosphate in the sludge is significantly higher than in this composite solution.

The modeling results for 40°C and 3 M NaOH were performed for three different leaching solutions (trials 1 through 3). The results for all three leaching solutions were similar, with sodium silicate ($Na_2SiO_3 \cdot 8H_2O$), uranyl hydroxide, and bismuth oxide all predicted to be at or near equilibrium. These results are also similar to the 1 M NaOH case described above. The only significant difference between the 3 M NaOH simulations and the 1 M NaOH simulation was in the closeness to saturation of the normal sodium phosphate phase, which was much closer to saturation in the 3 M NaOH case because of the higher Na concentration. In fact, if this phase were equilibrated with the solution, the phosphate concentration would increase only by a factor of three as opposed to a factor of 17 in the 1 M NaOH case. Hence, there is a much greater chance of reaching equilibrium with respect to sodium phosphate solubility limitations in the 3 M NaOH solutions in comparison with the 1 M NaOH solutions.

The modeling results for the 60°C and 1 M NaOH case showed only sodium silicate and uranyl hydroxide at or near equilibrium. All Bi-containing phases were predicted to be under-saturated, but bismuth oxide was predicted to be close to equilibrium. The increasing temperature also increased the potential solubility of the sodium phosphate phases. All sodium phosphate phases were predicted to be highly under-saturated. The potentially most stable phase shifted from the normal phosphate to the

octahydrate ($Na_3PO_4 \cdot 8H_2O$), which is consistent with the known stability of these phases as a function of temperature (see Figure 3.15a). The results for the same temperature but higher NaOH (3 M) were almost identical except that in addition to sodium silicate and uranyl hydroxide, the solutions were also predicted to be saturated with respect to bismuth oxide. Also, the increasing NaOH concentration shifted the sodium phosphate phase stability field slightly, causing the normal phosphate to be closer to equilibrium than the octahydrate, but both phases are still predicted to be significantly under-saturated.

The results at 80°C show only uranyl hydroxide at equilibrium or over-saturated in the 1 M NaOH solution and uranyl hydroxide and sodium silicate at equilibrium or over-saturated in the 3 M NaOH solution. The closest sodium phosphate-containing phase to equilibrium is now predicted to be the hexahydrate ($Na_3PO_4 \cdot 6H_2O$) owing to the lower water activity at the higher temperature. However, this phase is far from saturation at both NaOH concentrations.

The fact that the sodium phosphate phases are all highly under-saturated is supported by the analytical results that show a near 100% removal of phosphate from the leached sludge at all temperatures and NaOH concentrations.

Boehmite was the only phase positively identified in the solid phase following leaching at 40°C and 3 M NaOH. However, boehmite was predicted to be under-saturated in all leaching solutions by ESP. The presence of boehmite after leaching can be attributed to its slow dissolution kinetics which resulted in some undissolved boehmite remaining after the 24-h leaching time. The Cr concentrations observed in the leaching experiments are also of significant interest. If Cr is entered as Cr(III) into the model simulations, ESP predicts the formation of chromium oxyhydroxide (CrOOH) with a very low total Cr solubility ($\sim 10^{-8}$ M). However, Rai et al. (2002) have previously measured the Cr(III) concentrations in equilibrium with amorphous chromium hydroxide under basic conditions, and these measured concentrations are in reasonable agreement with the final (24-hr) chromium concentrations measured by Lumetta et al. (2009a), even though the temperature ranges from 40°C to 80°C (see Figure 3.17). This correspondence indicates that the final chromium concentrations in the leaching solutions could be limited by amorphous chromium hydroxide. Unfortunately, the thermodynamic data developed in Rai et al. (2002) are not in the ESP database.

Group 1 Test Material, Bismuth Phosphate Sludge: Summary

Thermodynamic modeling of the Group 1 test material (actual bismuth phosphate sludge) indicated that the phosphate concentration in the supernatant is potentially limited by the formation of the sodium phosphate-sodium fluoride double salt. The wash solution removes this readily soluble phase. Adding base during leaching causes a clear shift in equilibrium away from any possible bismuth phosphate equilibrium to stability with respect to bismuth oxide or bismuth hydroxide. All sodium phosphate phases were predicted to be under-saturated, which agrees with the experimental observation that the phosphate was readily leachable. Adding high concentrations of NaOH did not appear warranted because it did not increase the dissolution of phosphate from the waste and only increased the saturation level relative to sodium phosphate phases. This also is consistent with the results of the parametric testing done in this work with the $BiPO_4$ sludge simulant.

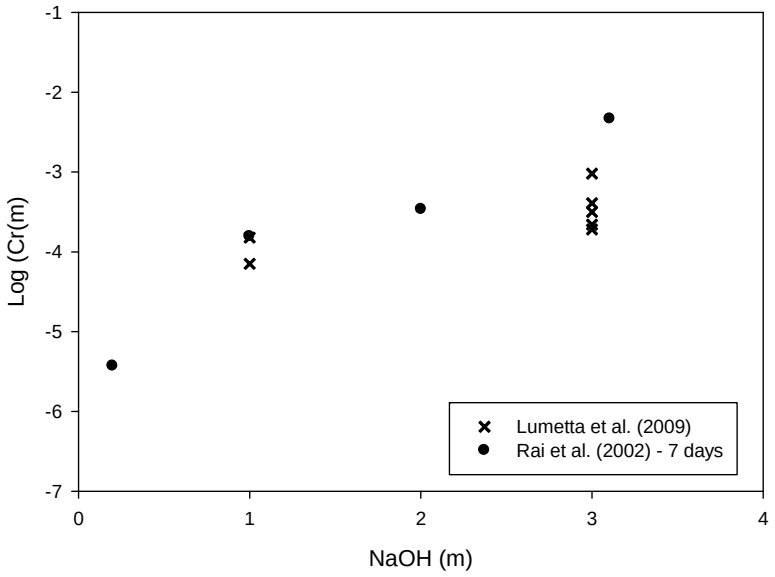

Figure 3.17. Experimental Cr Concentrations in NaOH Solutions. Data of Rai et al. (2002) for solutions in contact with amorphous Cr(III) hydroxide at different equilibration times and 25°C. Data of Lumetta et al. (2009a) in NaOH leaching solutions in contact with bismuth phosphate sludge at various temperatures and an equilibration time of 24 hours.

3.4.2.1.2 Group 2 Test Material—Bismuth Phosphate Salt Cake

Lumetta et al. (2009a) also report the analysis of salt cake supernatant solutions from dissolving bismuth phosphate saltcake, washed solids, and solutions generated from caustic leaching of those solids. The analytical data used in these simulations for supernatant and washed solids were taken from Table 4.6 of Lumetta et al. 2009a and that for the leached sludge solids were taken from Appendix J of that report.

Supernatant and Composite Washing Solution

Model simulations using the supernatant concentrations indicated that the supernatants were either in equilibrium or over-saturated with respect to gibbsite, bismuth oxide, and the sodium fluoride-sodium phosphate double salt [$Na_7F(PO_4)\cdot 19H_2O$]. In addition, both the sodium sulfate-sodium fluoride double salt ($Na_2SO_4\cdot NaF$) and sodium fluoride (NaF) are at or nearly in equilibrium. Sodium silicate ($Na_2SiO_3\cdot 8H_2O$) is also predicted to be over-saturated. However, in this case, if the formation of this phase is suppressed, the model predicts the formation of sodium aluminosilicate (specifically $Na_2Al_2Si_3O_{10}\cdot 2H_2O$). In these solutions, the insoluble fluoride compounds are the key solubility-limiting phases in determining the aqueous concentrations of fluoride, phosphate, and possibly sulfate in the supernatant. These relatively soluble phases, along with any gibbsite, should be removed to allow the dissolution of significant concentrations of phosphate.

In the case of the composite washing solution, the results are entirely different for the Group 2 material compared to the Group 1 material. The model predicts that the sodium fluoride-sodium phosphate double salt is still in equilibrium even after adding the wash solution. This is a result of the fact that, although the sodium concentration is much lower in the washing solution, the concentrations of both phosphate and fluoride increase, maintaining equilibrium with the sodium fluoride-sodium

phosphate double salt. These changes are also a partial validation of the presence of such a phase in the waste. Gibbsite was also predicted to remain in equilibrium with the composite washing solution, again indicating that this phase was not entirely removed by the washing step. The presence of a sodium aluminosilicate is also indicated by the modeling simulations, although the specific phase is now predicted as the lower sodium content sodium aluminosilicate (i.e., $NaAl_3Si_3O_{10}(OH)_2$) than in the supernatant solution. If maximum analytical detection limit values are used in the model simulations for U, Bi, and Ca, the predicted stable phases are uranyl hydroxide, bismuth oxide, and fluoroapatite.

Analysis of the washed solids by XRD, SEM-EDS, TEM, and vibrational spectroscopy (Lumetta et al. 2009a) indicated the possible presence of several phases in the washed Group 2 solids, including gibbsite, nitrate cancrinite, dorfmanite ($Na_2HPO_4 \cdot 2H_2O$), amorphous ferric phosphate, sodium autunite ($NaUO_2PO_4 \cdot 3H_2O$), and possibly urancalcarite [$Ca(UO_2)_3CO_3OH \cdot H_2O$]. The presence of both gibbsite and a sodium aluminosilicate is also supported by the model predictions. However, the current MSE thermodynamic database does not contain data for aluminosilicates with substituted anions such as nitrate, carbonate, etc. that can be present in the bismuth phosphate saltcake waste. This limitation is addressed in Section 3.4.3. Dorfmanite is predicted to be under-saturated by the thermodynamic model. However, since there was no experimental pH measurement, this prediction is primarily based upon a calculated pH value of ~12, which places the solutions in the stability field of the normal phosphate rather than dorfmanite. The ESP model also does not have thermodynamic data for amorphous ferric phosphate, sodium autunite, or urancalcarite. In fact, it should be recognized that the ESP modeling capability in general is not very comprehensive for actinide species and solids. Fortunately, we (Felmy et al. 2005) have previously developed accurate thermodynamic data for sodium autunite and included these data in the database of our thermodynamic model GMIN (Felmy 1995). If this thermodynamic model is used to analyze the wash solutions along with the estimated pH (11.9) from the ESP simulation, the results indicate that sodium autunite is slightly under-saturated. However, if the pH is lowered to only 11.4, sodium autunite is predicted to be the equilibrium phase. This lower pH would also be more consistent with the possible presence of dorfmanite indicated above.

Parametric Leaching Studies

Leaching studies were performed on the Group 2 test material at three different temperatures (60, 80, and 100°C) and at different concentrations of NaOH. The 60°C experiments were performed at 3 M NaOH, 80°C at 1 M, 3 M, and 5 M NaOH, and the 100°C experiments at 3 M NaOH. In all cases, possible phosphate containing precipitates, including the normal phosphate and the sodium phosphate-fluoride double salt, were significantly under-saturated and never were predicted to limit the solubility of phosphate. Uranyl hydroxide was predicted to form in all cases. Sodium silicate, specifically $Na_2SiO_3 \cdot 8H_2O$, was also predicted to be in equilibrium or oversaturated in all NaOH solutions with greater than 1 M NaOH. This phase was predicted to be soluble only in the 1 M NaOH solution at 80°C. Fluoroapatite was also predicted to be in equilibrium or oversaturated if the analytical detection limit values for Ca were used in the simulations. If the formation of sodium silicate was suppressed, no other aluminum-containing phases were predicted to become saturated.

XRD analysis of the solids following leaching indicated the possible presence of several phases, including cancrinite, hydroxyapatite, clarkeite [$Na(UO_2)O(OH)$], and possibly uranium dioxide (UO_2). The analysis also indicated that gibbsite was removed during the leaching process. The thermodynamic modeling supports the removal of gibbsite because this phase was under-saturated in all of the leaching solutions. The thermodynamic modeling also indicates that a calcium phosphate solid could be stable in

these systems, although the thermodynamics support the formation of fluoroapatite rather than hydroxyapatite. Thermodynamic data for clarkeite are not in the ESP model, and the solutions would need to be very reducing to allow the formation of UO_2, which seems very unlikely.

If the Cr is added as Cr(III), the ESP model predicts the formation of chromium oxyhydroxide with a very low solubility (10^{-9} to 10^{-10} M), which is very similar to the predictions of the leaching of the bismuth phosphate sludge (Group 1 test material). However, in the case of the bismuth phosphate saltcake, the data at lower hydroxide concentrations appear to be higher than the solubility of amorphous chromium(III) hydroxide measured by Rai et al. (2002), indicating the possible presence of significant concentrations of Cr(VI) species in the lower NaOH leaching solutions (see Figure 3.18). The more concentrated NaOH leaching solutions appear to be near equilibrium with amorphous chromium (III) hydroxide.

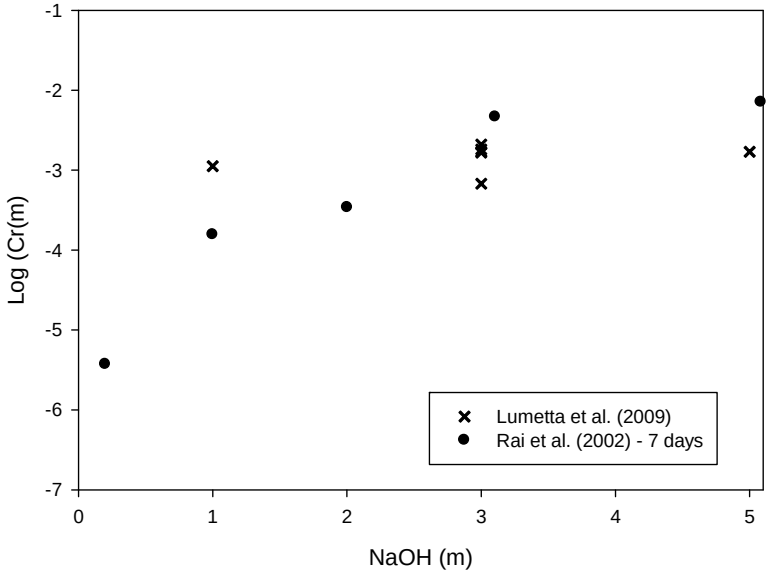

Figure 3.18. Experimental Cr Concentrations in NaOH Solutions. Data of Rai et al. (2002) for solutions in contact with amorphous Cr(III) hydroxide at early equilibration times and 25°C. Data of Lumetta et al. (2009a) in NaOH leaching solutions in contact with bismuth phosphate saltcake at various temperatures and an equilibration time of 24 hours.

Group 2 Test Material, Bismuth Phosphate Saltcake: Summary

In the case of the Group 2 test material (actual bismuth phosphate saltcake), the supernatant was at or near equilibrium saturation with respect to gibbsite, several fluoride-containing phases including the sodium fluoride-sodium phosphate double salt, and sodium aluminosilicate ($Na_2Al_2Si_3O_{10}\cdot 2H_2O$). The addition of wash solution did not completely remove these phases and gibbsite, the sodium fluoride-sodium phosphate double salt, and possibly sodium aluminosilicate are still predicted to be present in the waste solids. In addition, sodium autunite is possibly controlling the solubility of uranium in the washed saltcake. The caustic leaching solutions were all under-saturated with respect to all possible sodium phosphate solid phases, indicating that phosphate should have leached from the waste. However, the actual leaching solution did not show good phosphate removal. Lumetta et al. (2009a) hypothesized that the relatively poor phosphate removal could have resulted from the presence of

phosphate in insoluble hydroxyapatite. The thermodynamic modeling also indicates that calcium phosphate phases could be stable. Although here, fluoroapatite is predicted to be the stable calcium phosphate phase.

3.4.2.1.3 Group 1/2 Test Material—Blend of Bismuth Phosphate Sludge and Saltcake

Samples of the Group 1 and Group 2 test materials described above were blended to create a composite waste sample for further leaching studies. The original supernatant of the blended material was analyzed, and then the waste was subjected to series of caustic leaching, washing, and oxidative leaching steps. The analytical data are reported in Lumetta et al. (2009a).

Supernatant Analysis

Both a high solids and low solids slurry were prepared using the blended waste. The two slurries differed only in terms of the solid to liquid ratios. The supernatant was the same in both slurries. The analytical data used in these simulations were taken from Tables 5.2 and 5.10 of Lumetta et al. 2009a. Not surprisingly, thermodynamic modeling of the supernatant concentrations indicated saturation or possible equilibrium with solids phases that had been previously identified in the separate Group 1 or Group 2 test materials. The correspondence was most pronounced with respect to the Group 2 test material, which in general showed the presence of more soluble solid phases. In fact, all of the possible phases identified as possible equilibrium phases in the Group 2 material, including gibbsite, bismuth oxide, uranyl hydroxide, the sodium fluoride-sodium phosphate double salt [$Na_7F(PO_4)\cdot 19H_2O$], $Na_2Al_2Si_3O_{10}\cdot 2H_2O$, the sodium sulfate-sodium fluoride double salt ($Na_2SO_4\cdot NaF$), and sodium fluoride (NaF), were predicted to be at or nearly in equilibrium with the supernatant. In addition, if Fe is included as Fe(III), and Ca is included at its maximum value (i.e., the method detection limit), then hematite and fluoroapatite are predicted to be thermodynamically stable. The only noted difference between the model simulations of the blended waste and the Group 2 test material was the possible importance of a manganese-containing phase (calculated to be a manganese aluminosilicate [$Mn_5Al_2Si_3O_{10}(OH)_8$] because of the somewhat higher Mn concentration in the blended supernatant.

Caustic Leach and Wash

The blended waste described above was then subjected to a series of caustic leaching and washing steps. The final caustic leaching step was performed starting at a total hydroxide concentration of 4.6 M and 25°C. The temperature was then slowly ramped up to 96°C where the leachate solution was maintained in contact with the solids for a period of 8 h. The liquid phase was analyzed at various reaction times and temperatures (see Table 5.15 in Lumetta et al. 2009a). Unfortunately, a complete analysis of anions, including nitrate and nitrite, was unavailable. Hence, the necessary charge balance was maintained in the simulations by adjusting nitrate to compensate for the anion imbalance, or sodium if excess anions (i.e., hydroxide) were present over the analytical sodium concentration.

At 25°C, the modeling results show near equilibrium with the normal phosphate, indicating that solid sodium phosphate phases are possibly still present, and they control the concentration of dissolved phosphate. Equilibrium with respect to the sodium fluoride-sodium phosphate double salt could not be evaluated because of the lack of analytical data for fluoride. However, adding the high-base concentration now results in a significant under-saturation with respect to gibbsite. This observation is not surprising because the Al concentration is lower in the leachate solution, and the hydroxide is much

higher than in the original supernatant. The sodium aluminosilicate solids are also predicted to be under-saturated.

At 40°C, the normal phosphate is predicted to be significantly under-saturated. This results from the much lower analytical value for phosphate in the solution analysis. The prediction of under-saturation with respect to sodium phosphate is in disagreement with the conclusions of Lumetta et al. (2009a), who hypothesized that the lower phosphate concentration results from equilibrium with respect to such phases. The only caveat to this conclusion is the possible, and even likely, presence of insoluble sodium fluoride-sodium phosphate. Unfortunately, analytical data for fluoride are unavailable to test this possibility. Aluminum also appears to be under-saturated with respect to both gibbsite and all aluminosilicate phases, even though the solution phase aluminum concentration has increased over the 25°C value.

The solution analyses reported at 76, 92, 97°C, and the final 8-h leach at 96°C all show similar results with respect to phosphate and aluminum concentrations. All possible phosphate-containing phases are under-saturated along with the aluminum hydroxides. However, aluminosilicate phases begin to approach saturation with the model predicting the formation of $NaAlSiO_4$. Unfortunately, the current thermodynamic data for the aluminosilicates in ESP are too uncertain for any definitive conclusions about such phases. Therefore, these data are being re-evaluated as part of this study (see Section 3.4.3). Iron oxide (hematite) and uranyl hydroxide are also predicted be in equilibrium or oversaturated in these leachate solutions.

Analysis of the final leached dewatered slurry is also informative because complete anion analysis is available (see Table 5.18 in Lumetta et al. 2009a). The results indicate that several phases, originally predicted to be in equilibrium with the blended waste supernatant, are either still in equilibrium or very close to saturation. These phases include bismuth oxide, uranyl hydroxide, the sodium fluoride-sodium phosphate double salt, $NaAlSiO_4$, $Na_2Al_2Si_3O_{10}{\cdot}2H_2O$, the sodium sulfate-sodium fluoride double salt ($Na_2SO_4{\cdot}NaF$), and sodium fluoride (NaF). The normal phosphate is also predicted to be close to saturation. These results support the contention in Lumetta et al. (2009a) that the increased sodium concentration and lower temperature could have caused the re-precipitation of phosphate that was originally released from the waste.

Following caustic leaching, the slurry was washed five times with solutions with decreasing NaOH concentration until the free hydroxide concentration was less than 0.25 M. Modeling of the wash solutions was hindered by the absence of complete anion analysis for the first four wash solutions. Hence, it was not possible to assess equilibrium with respect to any fluoride-containing phase in these solutions. Nevertheless, the results showed some interesting trends. The first wash solution was slightly under-saturated with respect to the normal phosphate, gibbsite, and sodium aluminosilicate ($Na_2Al_2Si_3O_{10}{\cdot}2H_2O$). However, the increasing sodium and phosphate concentration in the second wash solution brought both the normal phosphate and sodium aluminosilicate into either equilibrium or over-saturation. Gibbsite remained slightly under-saturated. In the third wash, the gibbsite saturation decreased slightly, the normal phosphate was under-saturated but close to saturation, and the sodium aluminosilicate phase was now highly under-saturated as a result of the reduced silica and sodium concentrations. The fourth wash solution showed a continuing trend of reduced saturation with respect to the normal phosphate and continued under-saturation with respect to gibbsite and sodium aluminosilicate, although the sodium aluminosilicate saturation actually increased slightly. Complete anion analysis was available for the fifth wash solution, which showed that at least by the fifth wash that all of the fluoride-containing phases were now under-saturated. The normal phosphate and all sodium

aluminosilicate phases were now also highly under-saturated. The only phases predicted to be in equilibrium were uranyl hydroxide, bismuth oxide, and hematite [if all Fe is included as Fe(III)].

Oxidative Leach and Wash

Following caustic leaching and washing, the blended waste was subjected to an oxidative leaching step using sodium permanganate ($NaMnO_4$) in basic (~0.2 M NaOH) solution. The oxidatively leached waste was then washed three times with 0.01 M NaOH to remove any leached Cr and other components. Unfortunately, it was not possible to analyze the oxidative leaching supernatant using the chemical model since neither complete anion analysis nor any measure of the base concentration (i.e., either free hydroxide or pH) were available (see Table 5.35 in Lumetta et al. 2009a). However, the base concentration was available for the first and second washes of the oxidatively leached blended waste, and complete analytical data were available for the third wash and the final permeate (Tables 5.36 through 5.39 and Table 5.42 in Lumetta et al. 2009a).

Chemical modeling of the first wash solution showed that equilibrium with a sodium aluminosilicate was still possible, calculated to be $NaAl_3Si_3O_{10}(OH)_2$. All sodium phosphate phases were calculated to be highly under-saturated. Gibbsite was predicted to be near saturation. In all subsequent washes and in the final permeate, both gibbsite and sodium aluminosilicate ($NaAl_3Si_3O_{10}(OH)_2$) were predicted to be saturated.

Finally, it is of interest to examine the results for the Cr concentrations by both caustic and oxidative leaching studies and compare these results with what would be expected from equilibrium with amorphous chromium (III) hydroxide (Figure 3.19). The results of the caustic leaching studies at base concentrations less than 3 M NaOH show higher Cr concentrations in solution than expected if the solutions contained Cr(III) in equilibrium with Cr(III) hydroxide, indicating that these solutions contained significant concentrations of soluble Cr(VI). However, the experimental results are very close to the expected equilibrium at NaOH concentrations greater than 3 M NaOH, indicating that amorphous Cr(III) hydroxide could be setting upper limits on the dissolved Cr concentrations in these solutions. All of the solutions that have undergone oxidative leaching show total Cr concentrations far in excess of what would be expected for chromium (III) hydroxide equilibria, clearly indicating that these solutions contain Cr(VI) as expected.

Group 1/2 Test Material, Blend of Bismuth Phosphate Sludge and Saltcake: Summary

In the case of the Group (1/2) blended waste, the supernatant appeared to be in equilibrium with essentially the same solid phases as were identified to be in equilibrium with the more soluble Group 2 test material. These phases included gibbsite, several fluoride-containing phases, and $Na_2Al_2Si_3O_{10}{\cdot}2H_2O$. This is expected because such soluble phases were present in both wastes, and they react relatively rapidly. During caustic leaching, all of these phases appear to become progressively more under-saturated as the temperature slowly increases. In the final 96°C leach solution, all sodium phosphate and aluminum hydroxide phases are under-saturated. Cooling and dewatering the slurry, however, results in an increased sodium concentration and the possible re-precipitation of the fluoride-containing phases and aluminosilicates. Washing this waste resulted in an apparent re-dissolution of these precipitates. The second wash in particular showed equilibrium with both the normal phosphate and sodium aluminosilicates. However, by the final fifth wash, all of these solids were predicted to have dissolved. The oxidative leach step and subsequent washes showed that both sodium

aluminosilicate and gibbsite could still be in equilibrium with the solutions even in the final wash step. However, it was very clear that adding permanganate increased the total chromium concentration far beyond any possible equilibrium with respect to chromium (III) hydroxide, indicating that this treatment was effective in converting Cr(III) to more soluble Cr(VI).

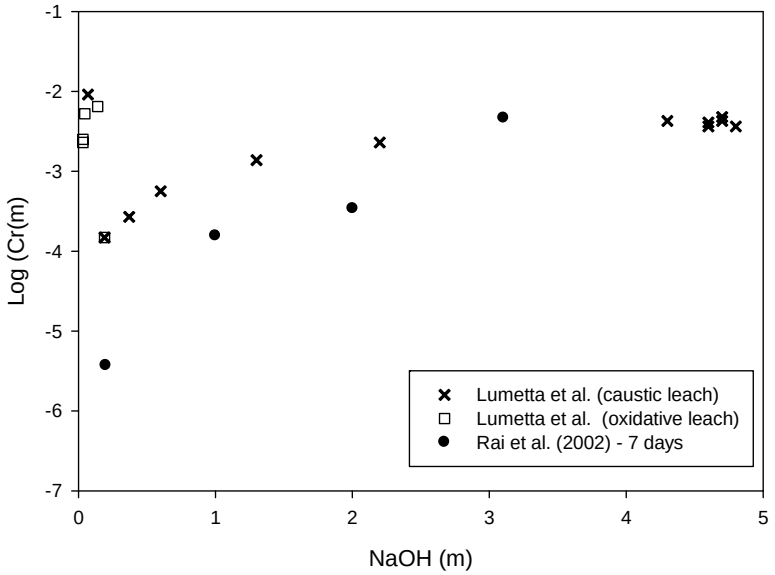

Figure 3.19. Experimental Cr Concentrations in NaOH Solutions. Data of Rai et al. (2002) for solutions in contact with amorphous Cr(III) hydroxide at early equilibration times and 25°C. Data of Lumetta et al. (2009a) in NaOH leaching solutions in contact with blended waste at various temperatures and an equilibration time of 24 hours.

3.4.3 Update of Thermodynamic Model

Overall, the thermodynamic model predictions satisfactorily agreed with the experimental data both in the simple systems examined (Section 3.4.1) and in the more complex actual waste tests examined (Section 3.4.2). However, during the course of these studies, certain potential limitations in the model became apparent. First, in examining the simple electrolyte solutions, the model gave very erroneous predictions for phosphate solubility in $NaNO_2$ solutions at high $NaNO_2$ (see Figure 3.15h). Since $NaNO_2$ can be present in high concentration in certain tank wastes, this inaccuracy was of some concern. Second, the thermodynamic model consistently predicted that a variety of sodium silicate or sodium aluminosilicate phases should form in both the leached bismuth phosphate sludges and supernatants. The formation of such phases can impact the leaching of phosphate by armoring the surface of particles and could even impact the final implementation of the sludge leaching process by coating tank walls or transfer lines. Hence, accurate predictions of these silicate reactions are also necessary. In collaboration with OLI Systems Inc., we have re-examined and improved the thermodynamic database for the Na_3PO_4-$NaNO_2$ system as well as for several sodium silicate and sodium aluminosilicate phases. These improvements to the thermodynamic database are described below.

The System Na_3PO_4-$NaNO_2$-H_2O

The ion-interaction parameters between PO_4^{3-} and NO_2^- were adjusted to correct for the large over-prediction in solubility. This refitting had the most impact in the region where the $Na_3PO_4 \cdot 8H_2O$ phase was stable (i.e., >5 M $NaNO_2$). The revised model predictions, Figure 3.20, show much better agreement with the existing experimental data. These new model parameters are in the latest version of the software (Analyzers 3.1.4 and ESP 8.2.4).

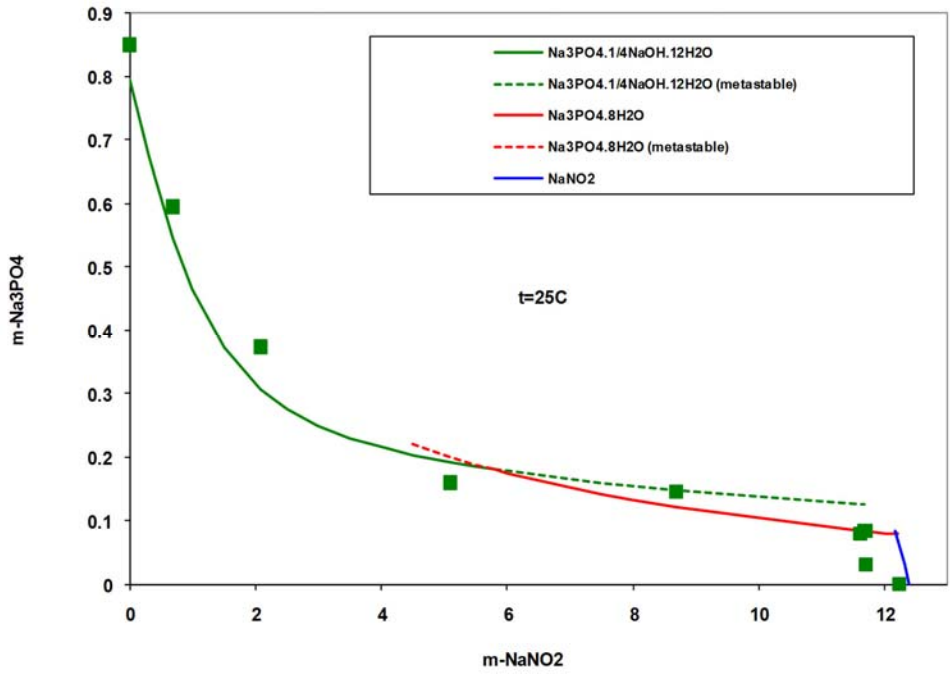

Figure 3.20. Experimental Data and Revised MSE Predictions of the Solubility Relations in the Na_3PO_4-$NaNO_2$-H_2O System at 25°C

*Sodium Silicate*s

The solubility data for four different potentially insoluble sodium silicate phases was re-evaluated: Na_2SiO_3, $Na_2SiO_3 \cdot 5H_2O$, $Na_2SiO_3 \cdot 9H_2O$, and $Na_3HSiO_4 \cdot 5H_2O$. All of the available experimental data were analyzed across the temperature range of 0 to 90°C. This re-evaluation was also necessary to establish an accurate foundation for the sodium-aluminosilicate parameterization. The ion-interaction parameters for Na^+-$HSiO_3^{3-}$, Na^+-$H_2SiO_3^{2-}$, OH^--$HSiO_3^{3-}$, and OH^--$H_2SiO_3^{2-}$ were also determined. An example of the agreement between model predictions and experimental data is given in Figure 3.21. The results show a region of relatively low silica solubility at low base concentration (~ 4 m NaOH), at least at low temperature. Such solubilities could be even lower in high $NaNO_3$ or other sodium-containing solutions.

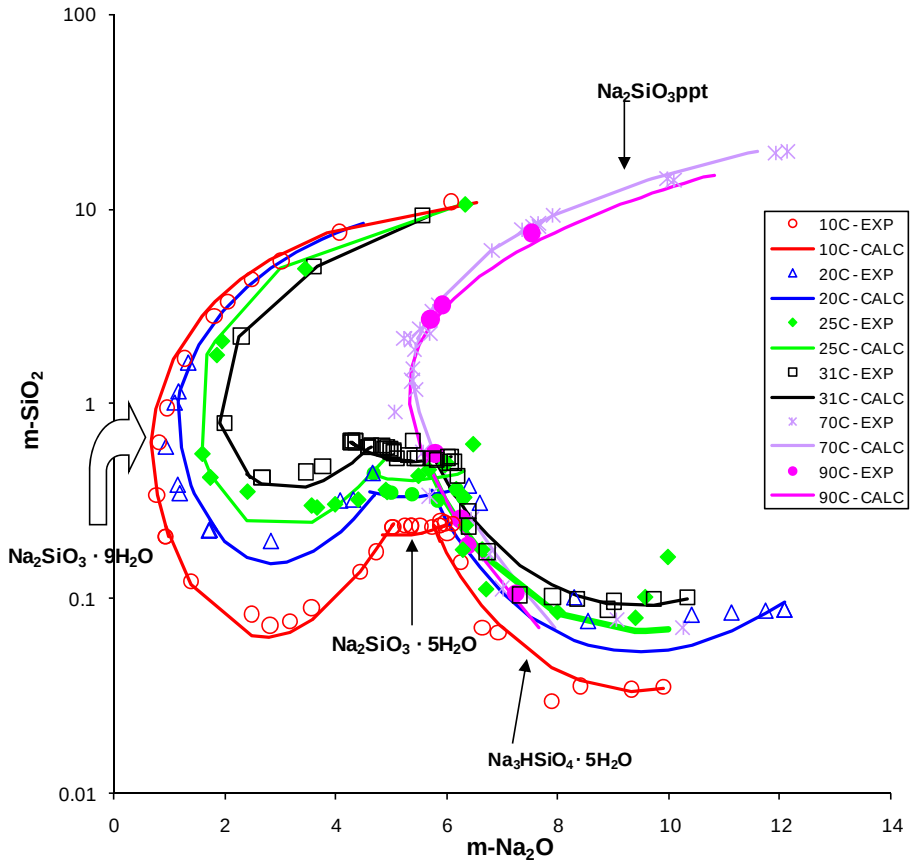

Figure 3.21. Experimental Data and MSE Predictions of the Solubility Relations in the Na_2O-SiO_2-H_2O System Across the Temperature Range 10 to 90°C

Sodium-aluminosilicates

The solubility data for five different potentially insoluble sodium aluminosilicate phases was re-evaluated: Hydrosodalite ($Na_8Al_6Si_6O_{24}(OH)_2{\cdot}2H_2O$), Zeolite A ($Na_6Al_6Si_6O_{24}{\cdot}12H_2O$), amorphous aluminosilicate gel ($Na_5Al_6Si_7O_{25.5}{\cdot}15.5H_2O$), and two hydrated forms of cancrinite containing carbonate ($Na_8Al_6Si_6O_{24}CO_3{\cdot}H_2O$ and $Na_8Al_6Si_6O_{24}CO_3{\cdot}H_2O$). The available experimental data were analyzed, extending from approximately 30° to as high as 250°C, depending upon the availability of the experimental data for specific systems. This analysis required the introduction of an $AlSiO_3(OH)_4^{3-}$ complex as well as adjustments to the ion-interaction parameters $Al(OH)_4^-$-$HSiO_3^{3-}$, Na^+-$AlSiO_3(OH)_4^{3-}$, OH^--$AlSiO_3(OH)_4^{3-}$, CO_3^{2-}-$AlSiO_3(OH)_4^{3-}$, and $Al(OH)_4^-$- $AlSiO_3(OH)_4^{3-}$. Examples of the agreement between model predictions and experimental data are given in Figure 3.22 through Figure 3.24.

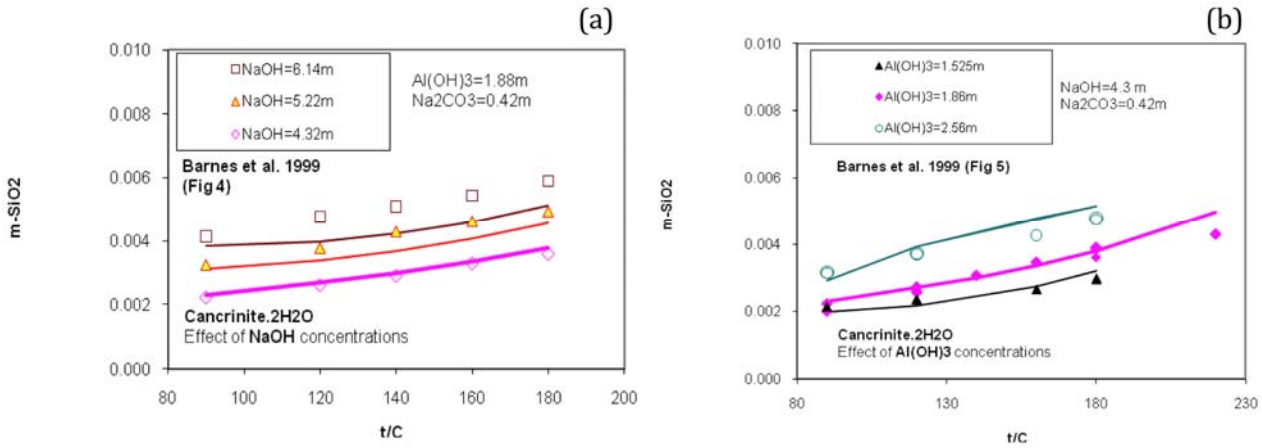

Figure 3.22. Experimental Data and MSE Predictions of the Solubility Relations in the $Al(OH)_3$-SiO_2-Na_2CO_3-H_2O at Temperatures >80°C: (a) Effect of NaOH, (b) Effect of $Al(OH)_3$

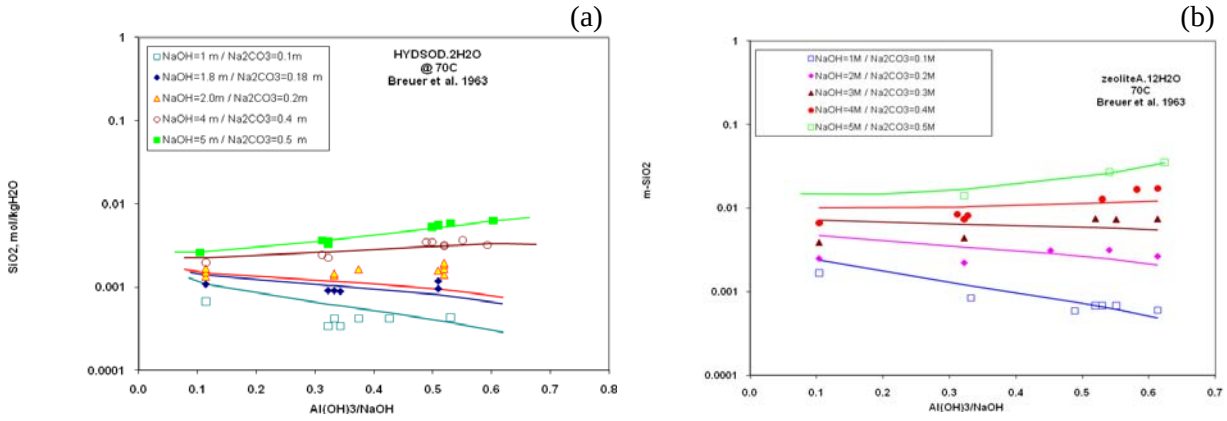

Figure 3.23. Experimental Data and MSE Predictions of the Solubility Relations in the $Al(OH)_3$-SiO_2-Na_2CO_3-H_2O at 70°C: (a) Hydrosodalite Solubility, (b) Zeolite A Solubility

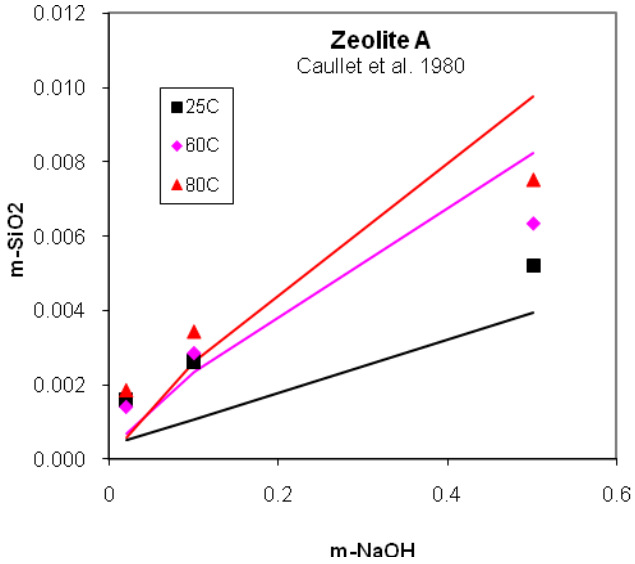

Figure 3.24. Experimental Data and MSE Predictions of the Solubility of Zeolite A as a Function of Temperature and NaOH Concentration

Interestingly, the predicted silica concentrations in equilibrium with the aluminosilicates are quite low (<0.01 m), even at higher temperatures. This finding strongly supports the observation of aluminosilicate precipitates in the leached bismuth phosphate supernatants and sludges. The new thermodynamic data for the sodium silicate and sodium aluminosilicate systems will be in the next release of the MSE version of ESP by OLI, Inc.

3.5 Sequential Phosphate Leaching and Calcium Oxide Treatment Tests

Four tests were conducted to couple the leaching of phosphate from the $BiPO_4$ sludge simulant with the lime treatment to recover the leached phosphate. The four tests represented different processing scenarios (Cases 1 through 4; Table 2.1). In Cases 1 and 2, it was assumed that the sludge solids had been prewashed to remove the bulk $NaNO_3$ from the waste. The difference between these two cases is that leaching was conducted at 25°C for Case 1 and 60°C for Case 2. In both Cases 1 and 2, the ratio of leaching solution to the initial mass of the $FePO_4 \cdot 3.4H_2O$ solid was 33 mL/g. Cases 3 and 4 assumed that the solids had not been prewashed, so considerable $NaNO_3$ would be present. In Case 3, the solution volume of the leachate solution was increased to 25 mL (202 mL/g $FePO_4 \cdot 3.4H_2O$ solid) so as not to exceed the sodium phosphate solubility limit. The higher temperature used in Case 4 (60°C) allowed the leachate solution volume to be reduced to 10 mL (83 mL/g $FePO_4 \cdot 3.4H_2O$ solid) while still having adequate PO_4^{3-} solubility.

The amount of $NaNO_3$ added to the $BiPO_4$ sludge simulant was based on the relative nitrate/phosphate ratio in an actual waste sample (Lumetta et al. 2009a). Likewise, in both tests performed, NaF and Na_2SO_4 were added in amounts expected based on the previous analysis of the actual waste. The amounts of these additional components added to the simulant are listed in Table 2.1.

The phosphate in each leachate solution was recovered by treating with CaO with a 4:1 ratio of calcium to phosphorus (assuming quantitative leaching of phosphate from the $BiPO_4$ occurred). Leached $BiPO_4$ simulant and leachate solutions were analyzed with ICP-OES. The percent of phosphate removed from the solid was calculated from the ICP-OES analysis and is presented in Table 3.3 for all cases, along with other elements of interest.

Table 3.3. Elemental Removal and Recovery from $BiPO_4$ Simulant and Leach Solutions, Respectively

		% & total mass (mg)[(b)] Removed—$BiPO_4$ Simulant		% & total mass (g)[(b)] Recovered—Lime Treatment		
Temp, C°	Nitrate Present?	Fe	P	Ca	Na	P[a]
22	No	<1, <0.1	82, 47	95, 190	<1, 3	>99, 47
22	Yes	<1, <0.1	89, 20	>99, 160	<1, 1	>99, 20
60	No	<1, <0.1	94, 56	98, 200	2, 7	>99, 56
60	Yes	<1, <0.1	93, 24	>99,140	<1, 0.2	>99, 24

(a) This is only the phosphorus recovery based on the lime treatment process. Since the lime treatment produced quantitative recovery (within error), the overall phosphorus recovery would be better indicated by the phosphorus percent removed from the $BiPO_4$ simulant.

(b) The total mass includes all calculations necessary to scale the values measured by ICP of the smaller analyzed sample to the total composition of the full sample.

Phosphate removal from the $BiPO_4$ simulant during leaching was the limiting step in phosphate recovery under the conditions examined here. At ambient temperature, phosphate removal was slightly higher when $NaNO_3$ was present; the reason for this is not clear at present. Heating the samples improved the recovery of phosphate both when nitrate was added and when it was not. This result is not consistent with the results of the parametric leaching experiments, which suggested that heating had no significant effect on phosphate removal from the $BiPO_4$ simulant (Section 3.2.2). The presence of fluoride and/or sulfate might have some influence on the $FePO_4/Fe(OH)_3$ metathesis reaction, leading to a temperature dependence. However, the effect of heating is relatively small; greater than 80% phosphate removal was achieved even at ambient temperature.

The results of the potentiometric titrations were consistent with previous examinations of the lime-treated aqueous phase when a 1:4 ratio of phosphate to calcium oxide was used. Two equivalents of hydroxide were released per every one equivalent of phosphate recovered. Table 3.4 compiles the titration results.

Table 3.4. Solution Composition of Leaching and Lime-Treated Aqueous Phases as Determined by Potentiometric Titrations

Leach Temp, C°	Nitrate Present?	mmol NaOH Released	OH^-:PO_4^{3-} eq.
22	No	3.6	2.3
22	Yes	1.4	2.2
60	No	3.7	2.4
60	Yes	1.3	2.0

The percent recovery of phosphorus in the calcium solids is in reasonable agreement with ICP results. Potentiometric titrations of the first phosphate kinetic test (Section 3.3.1) also showed a higher percentage of phosphate in the aqueous phase relative to the ICP analysis. Since the initial $BiPO_4$ solids that were initially washed had a higher phosphorus composition than the unwashed solids, the NaOH release was greater in systems where $NaNO_3$ was removed from the $BiPO_4$ simulant.

The FTIR spectra for the solids obtained after treating the leachate solutions with CaO are shown in Figure 3.25. The temperature had little effect on the observed FTIR spectral features. However, the presence of nitrate gave rise to significant spectral changes. In the absence of nitrate, the FTIR spectra suggest that the phosphate-containing product is hydroxyapatite or perhaps fluoroapatite, indicated by the $\nu_3(PO_4)$ band at 1030 cm^{-1} (although this band is shifted somewhat from that observed for commercially procured hydroxyapatite at 1016 cm^{-1}; see Figure 3.10). In the presence of nitrate ion, the $\nu_3(PO_4)$ band shifts to slightly higher energy at 1034 cm^{-1}. In addition, there are strong bands at 872 and 1407 cm^{-1}. These same bands are also observed in the cases in which nitrate is not present, but with much lower relative intensity. But because these bands appear in the absence of nitrate, they are not attributable to nitrate ion. The most likely explanation is that they are the $\nu_2(CO_3)$ and $\nu_3(CO_3)$ bands of $CaCO_3$ (Nakamoto 1986). Indeed, the FTIR spectrum of commercially procured $CaCO_3$ displayed similar bands at 873 and 1392 cm^{-1}, along with the $\nu_4(CO_3)$ band at 712 cm^{-1} (also seen in the solid residue obtained from the nitrate-containing leachates). The Raman spectral results also support the conclusion that $CaCO_3$ is present in the solids. FTIR examination of the starting CaO revealed similar spectral features with bands observed at 868, 1416, and 1462 cm^{-1}, so this might be the source of the calcium carbonate phase.

Figure 3.25 shows the Raman spectra for solids obtained after treating the leachate solutions with CaO. In all cases, a peak is observed at 963 cm^{-1}, which is identical to that for the $\nu_1(PO_4)$ band for commercially procured hydroxyapatite (Figure 3.10). Also seen in all cases, except that for treating the Case 1 leachate, is a band at 1087 cm^{-1}. This band is identical to that for the $\nu_1(CO_3)$ in $CaCO_3$. This assignment is also supported by the presence of a band at 283 cm^{-1} in the Raman spectra from Cases 2 through 4; this band is also seen in the spectrum of $CaCO_3$. The prominent peak at 614 cm^{-1} is currently unassigned. Thus, like the FTIR spectra, the Raman spectra suggest that the residual solids are mainly mixtures of hydroxyapatite and calcium carbonate, the latter presumably being formed from dissolution of CO_2 from the atmosphere into the leachate solutions. The reason why more relative $CaCO_3$ would form in the presence of nitrate is not obvious, but this might simply reflect the lower solubility of $CaCO_3$ in the presence of $NaNO_3$.

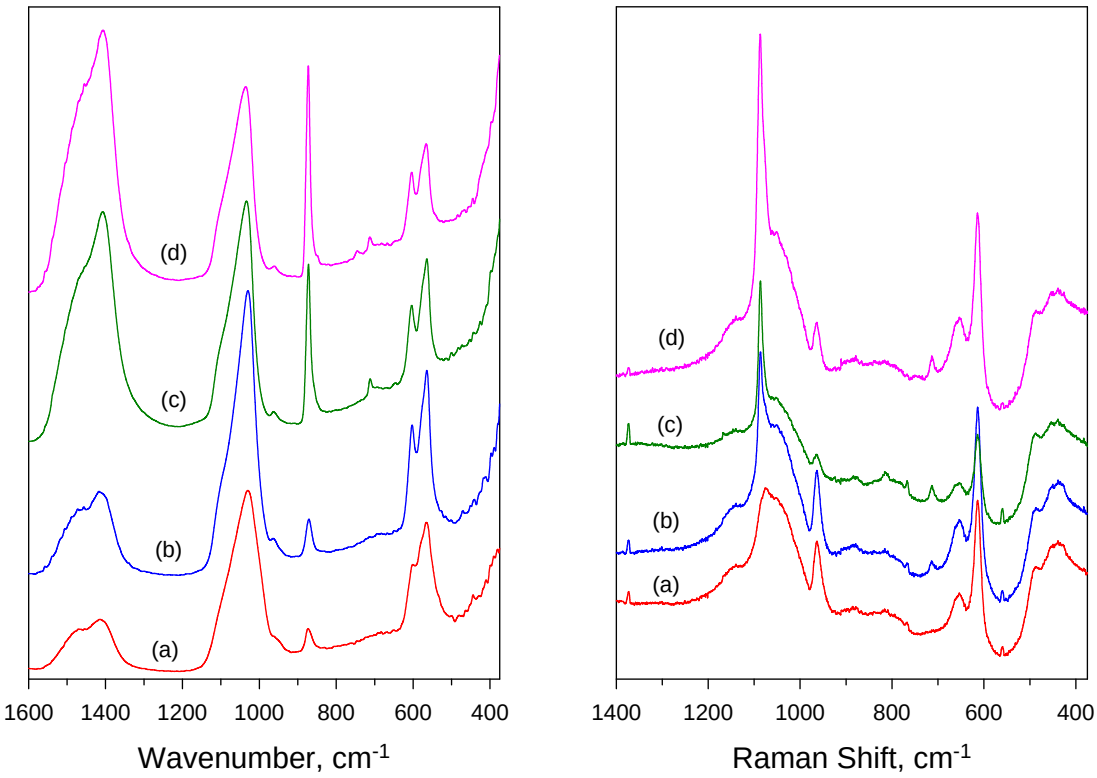

Figure 3.25. FTIR (left) and Raman (right) Spectra of Solid Residuals Remaining After Treatment of Phosphate-Containing Leachate Solutions With CaO: a) No Nitrate Added, Leached at Ambient Temperature, b) No Nitrate Added, Leached at 60°C, c) Nitrate Added, Leached at Ambient Temperature, and d) Nitrate Added, Leached at 60°C

4.0 Conclusions and Recommendations

Based on the results presented in this report, the approach shown in Figure 1.1 is a viable option for separating phosphate from the Hanford bismuth phosphate sludge waste before transferring this waste to the WTP for immobilization. The chemistry involved—metathesis of insoluble phosphate compounds to sodium phosphate and subsequent precipitation of calcium phosphate phases—is sufficiently robust that it can be implemented under a variety of conditions. The specific operating conditions can be chosen based on engineering requirements. For example, the entire process of caustic leaching, followed by treating the leachate solution with lime, can be performed at ambient temperature. Under such conditions, a relatively large solution volume would be used to maintain under-saturation of sodium phosphate. On the other hand, equipment requirements would be minimal because no heating equipment is required. Alternatively, the solution volume could be significantly reduced by heating the leachate solutions, which would increase the sodium phosphate solubility. This would have the advantage of decreasing the solution handling requirements, but would add complexity to the process since heating equipment would be required.

Another flowsheet parameter that must be further analyzed is whether to water-wash the sludge solids before performing the caustic leaching step. If washing is not required, the leaching step could be incorporated into the waste retrieval process, i.e., retrieve with 0.5 M NaOH. On the other hand, prewashing the sludge solids to remove soluble sodium salts would allow stricter control of the process product and reduce the amount of CaO required to precipitate the phosphate (by removing competing ions such a fluoride and sulfate). The methodology for collecting and handling the calcium phosphate product is another engineering aspect that needs to be evaluated. Possibilities include settle/decant, crossflow filtration, and rotary microfiltration. Thus, there are a number of engineering factors that need to be considered for optimizing the process. The site contractors should be engaged as early as possible to ensure a coordinated development effort for this phosphate management process.

Some outstanding technical issues that should be addressed in near-term (FY 2011) testing include:

1. Understanding the fate of ^{137}Cs and ^{99}Tc in the process. Ideally, these radionuclides will remain in the liquid phase after the CaO strike so that they are routed back to the tank farm (and ultimately to WTP).
2. Assessing the extent to which NaOH can be recycled in the process. If ^{137}Cs remains in the liquid phase after the CaO strike, this isotope will continue to build up with repeated recycling of the NaOH liberated during the calcium phosphate precipitation. Thus, the capability to recycle the NaOH might be constrained by "as low as reasonably achievable" (ALARA) considerations for operating the process. Additionally, if the sludge solids are not pre-washed to remove soluble sodium salts, $NaNO_3$ will also build up in the solution after repeated recycling, which could also constrain the capability to recycle the leaching solution.
3. Determining a suitable waste form for the calcium phosphate product. The calcium phosphate (mostly hydroxyapatite) solid formed upon treating the caustic leachate solution with CaO to removed phosphate will be an LAW material. Studies must be conducted to determine the best waste form option for this material.

4. Testing with actual tank waste. It is critical that testing with actual tank waste material be as performed to verify that the observations made with the simulant are also realized with the actual tank waste material.

We estimate that by the end of FY 2011, this technology will be at a Technical Readiness Level of 3 (DOE 2008).

5.0 References

Abduragimova RA and PF Rza-Zade. 1971. "Study of the (NaAlO2 + NaOH)-Na3PO4H2O System at 25 Degrees Celsius." *Russian Journal of Physical Chemistry, article 21B913*, pp. 179-185.

Certa PJ, GK Allen, TW Crawford, TM Hohl, KN Jordan, RA Kirkbride, and RL Lytle. 2008. *River Protection System Plan—Revision 3A*. Office of River Protection, Richland, Washington.

DOE—U.S. Department of Energy. 2008. *Technology Readiness Assessment (TRA)/Technology Maturation Plan (TMP) Process Guide*. Office of Environmental Management, Washington, DC.

Felmy AR. 1995. "GMIN, A Computerized Chemical Equilibrium Program Using a Constrained Minimization of the Gibbs Free Energy: Summary Report." In: *Chemical equilibrium and reaction models*, eds. RH Loeppert, AP Schwab, and S Goldberg. *Soil Science Society of America*, Division. p. 377-407. Madison, Wisconsin, American Society of Agronomy.

Felmy AR and GT MacLean. 2001. *Development of an Enhanced Thermodynamic Database for the Pitzer Model in ESP: The Fluoride and Phosphate Components*, PNWD-3120, WTP-RPT-018, Battelle--Pacific Northwest Division, Richland, WA.

Felmy AR, YX Xia, and ZM Wang. 2005. "The Solubility Product of $NaUO_2PO_4 \cdot \times H_2O$ Determined in Phosphate and Carbonate Solutions." *Radiochimica Acta* 93:401-408.

Foote HW and JF Schairer. 1930. "The System Na_2SO_4-NaF-NaCl-H_2O. I. The Ternary Systems with Water and Two Salts." *Journal of the American Chemical Society* 52:4202-4209.

Foote HW and JF Schairer. 1930. "The System Na_2SO_4-NaF-NaCl-H_2O. II. The Quaternary System at 25 and 35°." *Journal of the American Chemical Society* 52:4210-4217.

Kobe KA and A Leipper. 1940. "The System Trisodium Phosphate-Sodium Carbonate-Water." *Industrial and Engineering Chemistry* 32:198-203.

Kobe KA and A Leipper. 1988. "Alkali Metal Orthophosphates." In: *Solubility Data Series*, Vol. 31, p. 157. Oxford, Pergamon Press.

Korf DM and AM Balyasnaya. 1988. "Alkali Metal Orthophosphates." In: *Solubility Data Series*, Vol. 31, p. 139. Oxford, Pergamon Press.

Linke WF. 1965. *Solubilities of Inorganic and Metal-Organic Compounds : A Compilation of Solubiblity Data from the Periodical Literature*, American Chemical Society, Washington, DC.

Lumetta GJ, BM Rapko, J Liu, and DJ Temer. 1998. "Enhanced Sludge Washing for Pretreating Hanford Tank Sludges." In: *Science and Technology for Disposal of Radioactive Tank Wastes*, WW Schulz and NJ Lombardo, eds., Plenum Press, New York, pp. 203-218.

Lumetta GJ, LP Darnell, PA Garza, LR Greenwood, BM Oliver, DE Rinehart, DR Sanders, CZ Soderquist, T Trang-Le, MW Urie, and JJ Wagner. 2002. *Caustic Leaching of Hanford Tank T-110 Sludge*. PNNL-13956, Pacific Northwest National Laboratory, Richland, Washington.

Lumetta GJ. 2008. *Mechanism of Phosphorus Removal from Hanford Tank Sludge by Caustic Leaching.* PNNL-17257, WTP-RPT-173, Pacific Northwest National Laboratory, Richland, Washington.

Lumetta GJ, EC Buck, RC Daniel, K Draper, MK Edwards, SK Fiskum, RT Hallen, LK Jagoda, ED Jenson, AE Kozelisky, PJ MacFarlan, RA Peterson, RW Shimskey, SI Sinkov, and LA Snow. 2009a. *Characterization, Leaching, and Filtration Testing for Bismuth Phosphate Sludge (Group 1) and Bismuth Phosphate Saltcake (Group 2) Actual Waste Sample Composites*. PNNL-17992, WTP-RPT-166, Pacific Northwest National Laboratory, Richland, Washington.

Lumetta GJ, BK McNamara, EC Buck, SK Fiskum, and LA Snow. 2009b. "Characterization of High Phosphate Radioactive Tank Waste and Simulant Development." *Environ. Sci. Techol.* 43:7843-7848.

Mason CW and EB Ashcraft. 1939. "Trisodium Phosphate-Sodium Fluoride - Phase Studies and Analytical Methods." *Industrial and Engineering Chemistry* 31:768-774.

Mokretskii NP and EV Portyannikova. 1980. "Solubility in Na_2SO_4+2HF Reversible H_2SO_4+2NaF-H_2O System at 80-Degrees-C." *Zhurnal Neorganicheskoi Khimii* 25:1975-1980.

Morales JW, HR Galleguillos, and F Hernandez-Luis. 2007. "Solubility of NaF in NaF+NaX+H_2O (X = ClO_4 and NO_3) Ternary Systems and Density and Refractive Index of the Saturated Solutions at 298.15 K." *Journal of Chemical and Engineering Data* 52:687-690.

Morozova VA and EP Rzhechitskii. 1977. "Solubility in NaF-$NaHCO_3$-H_2O NaF-Na_2SO_4-H_2O and NaF-Na_2CO_3-H_2O Systems at 0 Degrees C." *Zhurnal Neorganicheskoi Khimii* 22:873-874.

Nakamoto K. 1986. *Infrared and Raman Spectra of Inorganic and Coordination Compounds*, 4th Ed., John Wiley & Sons, New York.

OLI Systems, Inc., The Environmental Simulation Program, Version 7.0.55, October 2, 2007.

Pabst A and WN Sharp. 1973. "Kogarkoite, a New Natural Phase in System Na_2SO_4-NaF-NaCl." *American Mineralogist* 58:116-127.

Protsenko PI, TI Ivleva, VV Rubleva, VA Berdyukova, and TV Edush. 1975. "Solubility and Properties of Solutions in Systems KNO_2-K_3PO_4-H_2O and $NaNO_2$-Na_3PO_4-H_2O at 25 Degrees." *Journal of Applied Chemistry of the USSR* 48:1104-1107.

Rai D, NJ Hess, LF Rao, ZC Zhang, AR Felmy, DA Moore, SB Clark, and GJ Lumetta. 2002. "Thermodynamic Model for the Solubility of $Cr(OH)_3$(am) in Concentrated NaOH and NaOH-$NaNO_3$ Solutions." *Journal of Solution Chemistry* 31:343-367.

Roslyakova ON, MR Petrov, and MI Zhikharev. 1979. "NaF-Na_3PO_4-H_2O System at 25-Degrees-C." *Zhurnal Neorganicheskoi Khimii* 24:206-208.

Selvaraj D, RK Toghiani, and JS Lindner. 2008. "Solubility in the Na+F+NO_3 and Na+PO_4+NO_3 Systems in Water and in Sodium Hydroxide Solutions." *Journal of Chemical and Engineering Data* 53:1250-1255.

Stark K and B Hultman. 2003. "Phosphorus Recovery by One- or Two-Step Technology with Use of Acids and Bases." In: *Proceedings of the International Water Association (IWA) Specialist Conference, BIOSOLIDS 2003*: *Wastewater Sludge as a Resource*. Trondheim, Norway, June 23-25, 2003, Dept. Land and Water Resource Engineering, Royal Institute of Technology, Stockholm, Sweden, pp. 281-288.

Steger E and W Schmidt. 1964. "Infrarotspektren von Sulfaten und Phosphaten." *Berichte der Bunsengesellshaft fur Physikalische Chemie* 68:102-109.

Toghiani RK, VA Phillips, and JS Lindner. 2005. "Solubility of Na-F-SO_4 in Water and in Sodium Hydroxide Solutions." *Journal of Chemical and Engineering Data* 50:1616-1619.

Zhikharev MI, MR Petrov, and ON Roslyakova. 1978. "$NaNO_3$-NaF-H_2O at 25-Degrees-C." *Zhurnal Neorganicheskoi Khimii* 23:1423-1424.

Distribution[(a)]

DOE-EM Office of Waste Processing
NP Machara
H Johnson
S Schneider

DOE Office of River Protection
BM Mauss

Washington River Protection Solutions
TL Sams
DJ Swanberg

Savannah River National Laboratory
M Hay
WR Wilmarth

Pacific Northwest National Laboratory
GJ Lumetta
JC Braley
JC Carter
MK Edwards
AR Felmy
PJ MacFarlan
O Qafoku
RA Peterson
BM Rapko
Information Release (pdf)

(a) Electronic distribution as pdf file.

Pacific Northwest
NATIONAL LABORATORY

U.S. DEPARTMENT OF
ENERGY

902 Battelle Boulevard
P.O. Box 999
Richland, WA 99352
1-888-375-PNNL (7665)
www.pnl.gov